Geochimica et Cosmochimica Acta Vol. 51, pp. 567–587

Constitutive mass balance relations between chemical composition, volume, density, porosity, and strain in metasomatic hydrochemical systems: Results on weathering and pedogenesis

GEORGE H. BRIMHALL and WILLIAM E. DIETRICH
Department of Geology and Geophysics, University of California, Berkeley, CA 94720, U.S.A.

(*Received June* 27, 1986; *accepted in revised form November* 25, 1986)

Abstract—Relations characterizing the chemical, physical, and mechanical changes resulting from metasomatic hydrochemical processes are developed using mass balance models which formally link chemical composition to bulk density, mineral density, volumetric properties, porosity, and amount of deformation (strain). Rigorous analysis of aqueous solute transport effects is then made possible in a variety of porous media flow environments including chemical weathering, pedogenesis (soil formation), diagenesis, ore deposition and enrichment, and metamorphism. Application of these linear constitutive relations to chemical weathering profiles shows that immobile and locally mobile chemical elements, with masses conserved on the scale of soil profiles, can be accurately identified from analysis of appropriate data arrays and then used as natural geochemical tracers to infer the nature and extent of hydrochemical weathering processes and volume changes during pedogenesis. Assumptions commonly made in the past about the supposed immobility of certain elements, *e.g.*, Ti and Zr, become unnecessary. Quantitative differentiation between the effects of residual and supergene fractionation is then easily made.

These methods are applied to Ni-rich laterites developed by weathering of ultramafic rocks, showing that during ordinary residual enrichment, Ni is concentrated by as much as 4× protolith peridotite concentrations. This occurs simply by silicate mineral dissolution and removal of chemical elements other than Ni (*e.g.*, Mg) with a corresponding reduction in saprolite density and increase in bulk porosity without significant deformation. In contrast, laterites with mineable concentrations of Ni which are similarly undeformed (such as the Nickel Mountain Mine in Riddle, Oregon) have experienced, in addition to residual enrichment, strong supergene enrichment by fractionation of ore elements between a leached zone from which Ni is extracted and a complementary enriched zone positioned farther along the direction of ground water flow.

Soil-forming processes in podzol chronosequences developed on sandy beach terraces of the Mendocino Coast of California involved soil column collapse of 60 percent by dissolution of silicate minerals in the albic horizon of Al and Fe leaching, and 70 percent dilation (expansion) in the overlying organic-rich layer by root growth. The amount of erosion based upon paleosurface reconstructions using the excess mass of Fe, Al, Pb, Ga, and Cu in the zone of supergene enrichment (spodic horizon) below the ground water table indicates that subsurface erosion by dissolutional collapse is three times that of surficial erosion.

Finally, using published chemical data for Ti, Zr, and Cr on major bauxite deposits in Australia where erosion rates are thought to be low, we infer that there may have been major amounts of dissolutional collapse to explain the upwards increase of detrital zircon and rutile in weathering profiles.

GLOSSARY OF SYMBOLS

Chemical elements

- i Index for immobile chemical elements.
- j Index for supergene elements which are locally mobile but are reprecipitated with the chemical system of interest.
- k Index for mobile elements.

Volume

- V_p Representative elementary volume of protolith.
- V_w Representative elementary volume after weathering.

Distance

- $B_{i,p}$ Original protolith thickness of zone enriched in residual element i.
- $B_{i,w}$ Thickness of zone enriched in residual element i.
- $B_{j,p}$ Original protolith thickness of zone enriched in supergene element j.
- $B_{j,e}$ Thickness of zone enriched in supergene element j.
- $L_{T_{j,p}}$ Total calculated thickness of protolith zone before deformation by leaching element j. Defined by Eqn. (4).
- $L_{T_{j,l}}$ Total thickness of zone leached of element j after deformation. Defined by $L_{T_{j,l}} = (\epsilon_{j,l} + 1)^* L_{T_{j,p}}$.
- $L_{T_{j,e}}$ Total current leached column height based upon mass balance of supergene element, j.

Density

- ρ_p Bulk density of protolith.
- ρ_w Bulk density of residually-weathered zone.
- ρ_l Bulk density of supergene leached zone.
- ρ_e Bulk density of supergene enriched zone.
- ρ_g^0 Average mineral grain density in protolith.
- ρ_g Average mineral grain density.
- $\rho_{g,e}$ Average mineral grain density in enriched zone.
- $\rho_{g,l}$ Average mineral grain density in leached zone.

Concentration

- $C_{i,p}$ Concentration of immobile element i in protolith (in wt.% or ppm).
- $C_{i,w}$ Concentration of immobile element i in weathered product.
- $C_{j,p}$ Concentration of supergene element j in protolith.
- $C_{j,e}$ Concentration of supergene element j in enriched zone.
- $C_{j,l}$ Concentration of supergene element j in leached zone.

Strain

$\epsilon_{i,w}$ Net strain determined using immobile element i in weathered zone.
$\epsilon_{i,e}$ Net strain determined using immobile element i in supergene enriched zone.
$\epsilon_{i,l}$ Net strain determined using immobile element i in supergene leached zone.

Porosity

n^0 Porosity of protolith.
n Porosity of weathered material.
n_e Porosity in supergene enriched zone.
n_l Porosity in supergene leached zone.

Mass

m_g^0 Total mass of mineral grains in representative elementary volume of protolith.
m_g Total mass of mineral grains in representative elementary volume of weathered material.

INTRODUCTION

ABUNDANCE PATTERNS of chemical elements in weathering profiles and paleosols serve as an informative though complex link between interrelated transport processes at the surface of the earth. These include geochemical, biological, climatological, hydrological, and geomorphic processes. Chemical analysis of depth profiles down through soils, saprolites, and ultimately into underlying rocks is often used to estimate mobility of elements during weathering (ESSON, 1983), and indirectly, to infer paleo-topography, and paleoclimate (BRIMHALL *et al.*, 1985; ALPERS and BRIMHALL, in press), as well as to debate evolution *versus* uniformitarianism in the composition of the earth's ancient atmosphere (VAN HOUTON, 1982; HOLLAND, 1984).

Until recently these inferences could in general only be made qualitatively or semi-quantitatively because analysis has rested on the assumption that certain constituents such as Ti or Zr remained immobile (ESSON, 1983) and can therefore be used as standards of comparison for chemical gains and losses of more mobile elements transported further along a fluid flow path. The term "witness oxide," *e.g.*, SiO_2, is used in this capacity in the Russian literature (RODE, 1970). Similar approaches have been used in metamorphic petrology (GRESENS, 1976), but have been based upon questionable assumptions such as volume for volume mineral replacement. Similarly, processes by which laterites and bauxites form have been viewed as isovolumetric (MILLOT, 1970), partly on the basis of textural preservation, convenience, and for lack of a more rigorous approach. A distinct improvement in determining chemical gains and losses of chemical elements came through consideration of rock density (MEYER *et al.*, 1968). Nevertheless, although rarely acknowledged explicitly, several other complications which could cause incorrect interpretation of the effects of metasomatism have largely been ignored. These include the effects of deformation, local variation of metasomatic products due to heterogeneities in protoliths and lateral fluid flow (fluid flow which is not parallel to the sampling profile). The latter two difficulties have been addressed in BRIMHALL *et al.* (1985), through use of geological mass balance models.

While a number of studies of weathering profiles have included consideration of physical properties such as bulk density (NIA, 1968; GOLIGHTLY, 1979), very few indeed have used full formal statements of mass balance relating chemical, physical, volumetric, and mechanical properties of weathering products to those of the protolith (BRIMHALL *et al.*, 1985). The physical properties discussed here include bulk density and porosity. Chemical properties considered are element concentration (wt.% or ppm) and average mineral density. Volumetric properties refer to the volumes of the subzones, *i.e.*, depleted or enriched parts of metasomatic systems. Mechanical properties refer to strain due to deformation, either through collapse or expansion. Formulation of explicit relationships between these properties is a substantial departure from past efforts. It will be shown here that it is no longer necessary to assume that certain chemical species are immobile index species with which to compute chemical gains and losses from normalized analyses.

This quantitative mass balance approach makes it then possible to use chemical elements in rocks and soils as useful geochemical tracers indicative of specific hydrochemical transport processes during weathering or supergene enrichment. For our purposes we will divide the behavior of chemical elements into three categories. Residual elements are those which are immobile and are not transported by metasomatic fluids during weathering. Consequently, they are either residually enriched as other species are removed in solution or are residually diluted as mobile elements become enriched through precipitation. In contrast, supergene elements—literally meaning "from above" in the case of descending unsaturated ground water flow—are those elements which are locally moved between a depleted source region or leached zone where depletion of these elements occurs and a complementary enriched zone or "blanket" where reprecipitation occurs farther along a flow line. Finally, mobile elements are those which are leached without secondary reprecipitation along the flow path and leave the chemical system of interest.

In certain instances in which chemical fractionation effects are very strong, it is possible simply on the basis of element concentration patterns to assign elements to one of these categories. More typically, however, rigorous identification of the behavior pattern requires consideration of the masses of elements contained in weathering products along a flow path. This involves more variables than chemical composition alone.

MASS BALANCE EQUATIONS

Simply stated, the mass of a chemical element in a given volume of rock or soil is given by the product

of rock volume, bulk density, and metal concentration. Earlier studies, *e.g.*, GRESENS (1967), while illustrating the relationships of composition to volume in metasomatic processes, did not fully develop the relationships of density to other variables such as porosity, grain density, and strain in the statement of mass conservation. We will demonstrate that this is a serious oversight in a number of applications, specifically those in which density and therefore porosity vary substantially during metasomatism.

Residual enrichment

Residual enrichment of immobile elements, indexed here on i, occurs by the removal of other, more soluble (locally mobile) species j, or completely mobile species k. This effect is shown graphically in Fig. 1 for a representative elementary volume. A list of symbols is given in the Glossary. In the absence of lateral fluxes, the mass of an immobile element (i) contained in the original protolith or protore (p) volume before weathering, is retained in the rock after weathering (w), as given by product of volume, concentration, and density in these two states (Eqn. 1).

$$V_p\rho_pC_{i,p} = V_w\rho_wC_{i,w} \tag{1}$$

The representative elementary volume terms in this expression are three-dimensional. In the context of evaluating geochemical profiles, however, this geometry may be simplified by consideration of only one dimension, that is, the vertical thickness of individual zones within a weathering profile (BRIMHALL *et al.*, 1985). By doing so, we are assuming the flow path of descending ground water has been essentially vertical over the few meters of exposed weathering column. In one dimension, Eqn. (1) may be rewritten as Eqn. (2) in which B represents the columnar height of an elementary representative volume of protore (p) and its weathered equivalent (w).

$$B_{i,p}\rho_pC_{i,p} = B_{i,w}\rho_wC_{i,w} \tag{2}$$

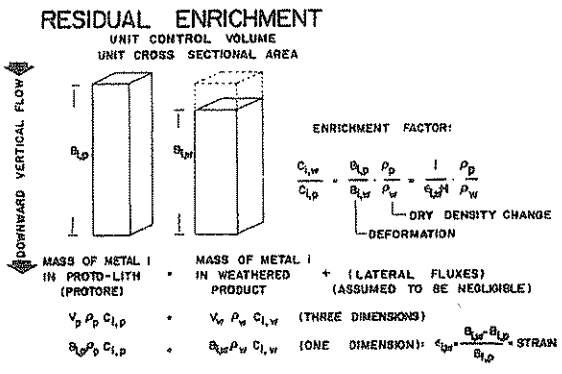

FIG. 1. Diagrammatic representation of mass conservation given as mass balance Eqns. (2) and (3) describing residual enrichment of immobile elements during chemical weathering shown in a one-dimension case of vertical flow. The mass of element i contained in protolith before weathering is equal to the mass in the weathered product. Strain during weathering is given as $\epsilon_{i,w}$ as shown.

The column height terms, $B_{i,p}$ and $B_{i,w}$ in Eqn. (2) may be eliminated by introducing the term $\epsilon_{i,w}$ for one-dimensional strain. In the case of residual weathering systems, we define $\epsilon_{i,w} = (B_{i,w} - B_{i,p})/B_{i,p}$, or change in length divided by original length, so that $B_{i,w} = B_{i,p}(\epsilon_{i,w} + 1)$. This strain term is indexed for any of a number of immobile elements i, implying that strain may be determined from a number of independent analyses. Substituting $B_{i,w}$ and cancelling the $B_{i,p}$ terms in Eqn. (2) leaves Eqn. (3).

$$\rho_pC_{i,p} = (\epsilon_{i,w} + 1)\rho_wC_{i,w} \tag{3}$$

In Eqn. (3) the density and concentration terms are easily measured directly, leaving strain, $\epsilon_{i,w}$, as the only unknown. This is an important analytical result as it provides a way to use chemical data to determine the amount of deformation in residual weathering profiles and soils. Strain in a weathering product may then be calculated from this expression of mass balance using the concentration of immobile elements and bulk density data relative to corresponding values in the protolith. Strain is positive for dilation and negative for collapse of the profile. Addition of material by aeolian deposition is not addressed in this present treatment.

Supergene enrichment

Mass balance equations for supergene enrichment include provision for the leaching of elements indexed on j, from a near-surface zone of thickness $L_{T_j,p}$ by ground water with reprecipitation in an underlying zone of enrichment of thickness $B_{j,e}$ such that the leached (l) and enriched (e) zones are complementary and together maintain overall mass conservation of the element j originally contained in the protore source region (Fig. 2). This differentiation of the protolith into two weathering subsystems in which fractionation of elements in the protore takes place between two discrete weathering zones requires a use of a two-zone notation instead of the single (w) notation previously derived for residual enrichment (Eqns. 1–3). The zones of leaching and enrichment of different supergene elements may not coincide. This necessitates the indexing of the thickness terms on elements j. Fractionation between the zones is described by Eqn. (4), a closed, chemical system, one-dimensional case without lateral fluxes or loss of element j through basal discharge.

$$\overset{(1)}{L_{T_j,p}\rho_pC_{j,p}} = \overset{(2)}{B_{j,e}\rho_eC_{j,e}} - \overset{(3)}{B_{j,p}\rho_pC_{j,p}} + \overset{(4)}{L_{T_j,l}\rho_lC_{j,l}} \tag{4}$$

In Eqn. (4) term 1 is the total mass of element j in the protore before leaching over the vertical column height, $L_{T_j,p}$. Term 2 is the mass of element j in the zone of enrichment which has a thickness $B_{j,e}$. Term 3 is the original mass of element j in the zone of enrichment with an undeformed height of $B_{j,p}$. The difference between terms 2 and 3 is the amount of element j added to the zone of enrichment by supergene flow and precipitation of secondary minerals containing element j. Term 4 is the mass of element j in a leached state, either present now in the geochemical profile or eroded away from the surface.

Definition of net strain, in this case for each of the two subsystems, simplifies Eqn. (4) by eliminating $B_{j,e}$ and $L_{T_j,l}$. We define strain in the enriched zone as ϵ_e where $\epsilon_{j,e} = (B_{j,e} - B_{j,p})/B_{j,p}$ and strain in the leached zone as $\epsilon_{j,l}$ where $\epsilon_{j,l} = (L_{T_j,l} - L_{T_j,p})/L_{T_j,p}$. Solving each of these equations for strain and substituting back into Eqn. (4) gives Eqn. (5), the overall mass balance equation for supergene systems.

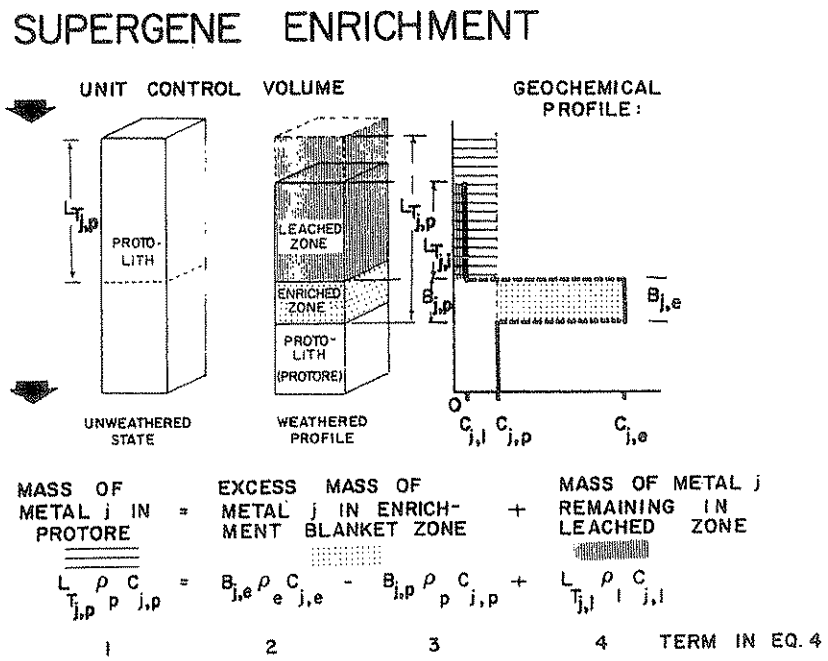

FIG. 2. Diagrammatic representation of one-dimensional mass balance Eqn. (4) for vertical supergene metal transport and secondary enrichment. Mass of element j leached is equal to the mass of j fixed in the underlying zone of secondary enrichment in this closed chemical system model in which a protolith volume becomes differentiated into two related parts. The uppermost subsystem is leached in element j, and the lower subsystem positioned further along a ground water flow line becomes enriched in j. Two strain terms are necessary. In the leached zone $\epsilon_{i,l} = (L_{T_{j,l}} - L_{T_{j,p}})/L_{T_{j,p}}$ and in the enriched zone $\epsilon_{i,e} = (B_{j,e} - B_{j,p})/B_{j,p}$.

$$L_{T_{j,p}}\rho_p C_{j,p} = B_{j,p}((\epsilon_{i,e}+1)\rho_e C_{j,e} - \rho_p C_{j,p}) - L_{T_{j,p}}(\epsilon_{i,l}+1)\rho_l C_{j,l} \quad (5)$$

Eqn. (5) describes a composite chemical system closed with respect to element j; that is, all of the element removed from the zone of leaching is ultimately fixed in the enrichment zone. This has been shown to be a geologically reasonable assumption in earlier studies (BRIMHALL *et al.*, 1985; CUNNINGHAM, 1984) in which the aqueous solubility of secondary mineral precipitates such as copper sulfides is so low that the basal discharge fluids contain little if any supergene leachates below the enrichment zone of the same element. We will show that for a variety of elements this assumption appears valid. While the variables in Eqn. (5) probably vary with time, mass conservation applies throughout the weathering history of a chemical profile, so that Eqn. (5) is valid at any point in time, even when substantial erosion has occurred (BRIMHALL *et al.*, 1985) and expresses the net redistributive effects of a supergene element. Note that it is immobile elements i that are used in the strain terms for supergene enrichment of mobile elements j.

EQUATIONS FOR ENRICHMENT FACTORS IN NON-DIMENSIONAL FORM

Separation of variables

In order to use metals as natural geochemical tracers with which to distinguish between various weathering mechanisms discussed, it is advantageous to separate chemical effects in mass balance expressions from those involving physical, volumetric, and mechanical variables.

Non-dimensional form of constitutive relations

We now proceed to derive mass balance expressions in non-dimensional (ratio) form. This is useful for two reasons. First, errors in the analysis are reduced, since changes in chemical, physical, and mechanical properties are expressed as ratios of the present values to those of the protolith. Measurement errors are similar on all types of samples and therefore would tend to cancel. Second, analytical solutions to mass balance equations in ratio form automatically scale physiochemical effects in each site with respect to the initial properties of that specific system. Thus weathering paths originating from even very different protoliths may be compared.

Residual enrichment

Rearrangement of Eqn. (3) provides a useful non-dimensional form of the equation of mass balance describing the overall chemical effects of residual enrichment (Eqn. (6)).

$$\frac{C_{i,w}}{C_{i,p}} = \frac{B_{i,p}}{B_{i,w}}\frac{\rho_p}{\rho_w} = \frac{1}{\epsilon_{i,w}+1}\frac{\rho_p}{\rho_w} \quad (6)$$

(1) (2) (3)

Term 1, expressed here as a unitless (non-dimensional) enrichment factor, is the ratio of concentration of metal i in the weathered product divided by the concentration of i in the protore. This term reflects the change in chemical composition of the system. Term 2 is a function of the amount of net accumulated strain in the column and hence relates to the mechanical effects of metasomatism. If there is no deformation, this term is unity, implying that the rate of increase of the enrichment factor with density ratio change occurs with a slope of one. Term 3 is the density ratio of the protore to that of the weathered material and is taken to be the main physical variable of interest. Notice that there is no explicit statement of the volumetric properties of the system as no fractionation into chemical subsystems occurs in residual enrichment. While the density ratio, Term 3, is easily measured, its interpretation is facilitated by transforming it into variation in porosity.

Porosity is defined as the ratio of void volume to total volume and is determined in soils and rocks by Eqn. (7), where ρ_w and ρ_g are bulk sample and average mineral grain densities, respectively, of weathered material.

$$n = 1 - \frac{\rho_w}{\rho_g} \tag{7}$$

Solving Eqn. (7) for ρ_w and substituting into Eqn. (6) gives

$$\frac{C_{i,w}}{C_{i,p}} = \overset{(1)}{\frac{1}{\epsilon_{i,w}+1}} \overset{(2)}{\frac{\rho_p}{\rho_g}} \overset{(3)}{\frac{1}{1-n}} \overset{(4)}{}. \tag{8}$$

In Eqn. (8) it is clear that, as in Eqn. (6), the residual enrichment factor (term 1) for an immobile element i can be interpreted as a function of a single controlling variable, in this case porosity (n) or, more precisely, $1/(1-n)$ (term 4). That is, as the porosity n increases, $1/(1-n)$ increases as well, causing the residual enrichment factor to grow with a rate determined by the amount of deformation of the system and mineralogic change given by terms 2 and 3, respectively. By using $1/(1-n)$ instead of n, the enrichment factor varies linearly with density ratio.

Supergene enrichment

Incorporating definitions of the two net strain terms in a differentiated supergene hydrochemical system, Eqn. (5) can be solved for the supergene enrichment factor as

$$\frac{C_{j,e}}{C_{j,p}} = \overset{(1)}{\frac{(L_{T_j,p}+B_{j,p})}{B_{j,p}}} \overset{(2)}{\frac{1}{(\epsilon_{i,e}+1)}} \overset{(3)}{\frac{\rho_p}{\rho_e}} \overset{(4)}{-} \overset{(5)}{\frac{L_{T_j,p}}{B_{j,p}}} \overset{(6)}{\frac{C_{j,l}}{C_{j,p}}} \overset{(7)}{\frac{(\epsilon_{i,l}+1)}{(\epsilon_{i,e}+1)}} \overset{(8)}{\frac{\rho_l}{\rho_e}}. \tag{9}$$

In Eqn. (9) the supergene enrichment factor, term 1, is a considerably more complex function that in the case for residual enrichment (Eqn. (6)) and involves the ratio of the leached zone thickness to the thickness of the zone of enrichment in terms 2 and 5. As in Eqn. (6) a strain term in the enriched zone appears (term 3) in a product with the density ratio of the protore to enriched zone, ρ_p/ρ_e (term 4). Terms 2, 5, 6, 7, and 8 have no counterparts in the residual case (Eqn. (6)).

Terms 1 and 6 in Eqn. (9) express the chemical compositions of the two related subsystems. Terms 2 and 5 express the volumetric properties of the leached and enriched systems. Terms 3 and 7 are functions of net strain in the enriched and leached subsystems and express changes in the mechanical properties. Terms 4 and 8 give the physical properties. Taken as a whole, Eqn. (9) describes the redistribution of a supergene element j from a protore state into the present complementary leached and enriched zones which together constitute a fractionated closed chemical system with respect to element j. Fractionation of element j is affected by term 2 which has a strong focusing effect on metal distribution from the fact that leached zones are generally much thicker than zones of enrichment. Consequently, the rate of increase of the enrichment factor (term 1) with density change (term 4) is much greater than unity, the slope derived for non-deformational residual enrichment (Eqn. (6)). This is one major difference between supergene and residual enrichment.

Comparison of Eqns. (6) and (9) shows that the expressions for enrichment factors of residual and supergene processes are similar in form when the density ratio of protore to enriched material is viewed as the independent physical variable. The expressions differ mainly in the term for slope, that is, rate of change of enrichment factor with density ratio increase. In residual enrichment the extent of fractionation of an immobile species is controlled simply by physical (density or porosity) and mechanical (strain) variables in a single hydrochemical system. In contrast, supergene fractionation involves variation in physical, chemical, mechanical, and volumetric properties of two subsystems. The supergene enrichment expression (Eqn. (9)) therefore contains an additional term describing the amount of leaching of mobile elements from the source region (term 6). This is a second difference in supergene and residual fractionation systems.

Bulk density terms in Eqn. (9) are transformed in terms of porosity in Eqn. (10):

$$\frac{C_{i,e}}{C_{j,p}} = \overset{(1)}{\frac{(L_{T_j,p}+B_{j,p}}{B_{j,p}}} \overset{(2)}{\frac{1}{(\epsilon_{i,e}+1)}} \overset{(3)}{\frac{\rho_p}{\rho_{g,e}}} \overset{(4)}{\frac{1}{1-n_e}} \overset{(5)}{} - \overset{(6)}{\frac{L_{T_j,p}}{B_{j,p}}} \overset{(7)}{\frac{C_{j,l}}{C_{j,p}}} \overset{(8)}{\frac{(\epsilon_{i,l}+1)}{(\epsilon_{i,e}+1)}} \overset{(9)}{\frac{\rho_{g,l}}{\rho_{g,e}}} \overset{(10)}{\frac{(1-n_l)}{(1-n_e)}}. \tag{10}$$

In Eqn. (10) $\rho_{g,e}$ and $\rho_{g,l}$ are the average mineral grain densities in the enriched and leached zones, respectively. It is clear that the supergene enrichment factor increases with volumetric fractionation (term 2), collapse ($\epsilon_{i,e}$, term 3), growth of low density secondary minerals (term 4), and increasing porosity (term 5) in the enriched zone. The enrichment factor also increases with the following changes in the source region or leached zone: continued leaching (term 7), collapse (term 8), growth of high density minerals (term 9), and porosity reduction (term 10).

RELATIONSHIPS OF RESIDUAL AND SUPERGENE ENRICHMENT

As is evident in Eqns. (8) and (10), residual and supergene enrichment have a number of factors in common. In fact, it can be shown that residual enrichment (Eqn. (8)) is related to supergene enrichment (Eqn. (10)) in the limiting case in which the extent of leaching of a mobile element j is negligible, *i.e.*, $L_{T_j,p}$ approaches zero, and Eqn. (10) reduces to Eqn. (8) describing simple residual enrichment.

In residual enrichment, any one of the following effects enhance enrichment: increase in rock porosity through dissolution of minerals containing mobile elements, formation of low density minerals, and collapse of the zone of enrichment. In addition to these factors, however, supergene enrichment involves volumetric fractionation of elements between two subsystems. Hence, the relative sizes of these subsystems expressed as $L_{T_j,p}/B_{j,p}$ and the extent of leaching in the source region $C_{j,l}$ is important as well and may even dominate the enrichment factor.

The main advantage of our methods is that, for the first time, constitutive mass balance equations provides a means to determine rigorously the importance of a number of fundamental physiochemical processes in complex surficial phenomena.

SELECTION OF FIELD SITES

For application of our methods we have selected two types of weathering systems differing greatly in the nature of the protolith: one is composed of non-porous, highly competent ultramafic rocks and the other of highly porous and poorly consolidated granular beach sand. Weathering of the former yielded laterites, of the latter, podzols. Lateritic soils were chosen because they are so broadly distributed worldwide and are among the most well-studied of all soils due to their considerable economic and agricultural value (WILSON, 1983;

GOLIGHTLY, 1979, 1981; GRUBB, 1979); podzols were selected because of the extreme state of hydrochemical fractionation by leaching of metals (for example, Fe and Al) from the near surface environment and reprecipitation in a deeper enriched zone. Finally, since the two types of protoliths vary considerably in terms of their initial porosity and rock strength, the opportunity exists of evaluating the extent of deformational processes attending chemical weathering of two very distinct materials.

Two field sites in Oregon were selected to investigate lateritic weathering of ultramafic protores through application of the two mass balance models: residual and supergene enrichment. From the distribution of data points in the coordinate system relevant to Eqns. (6) and (9), we can deduce the mechanisms of chemical weathering, including an estimate of the amount of deformation, assuming that lateral flow fluxes were negligible. Nickel was chosen for this mass balance study as it is an important ore metal and has an abundance high enough to be measured accurately. These specific field sites were chosen as being ideal for contrasting residual and supergene enrichment; otherwise there is an overall similarity of protolith rock type, topography, and presumed age of lateritic weathering between these two nearby laterites (RAMP, 1978).

One site, the Eight Dollar Mountain laterite (RAMP, 1978) is one of over one hundred similar Ni- and Co-rich laterite prospects (HOTZ, 1964; RAMP, 1978) developed on ultramafic portions of a major ophiolite in southern Oregon and northern California (the Josephine Peridotite). The Nickel Mountain Mine, a much larger and higher grade deposit (CUMBERLIDGE and CHASE, 1968), was chosen for our study as published descriptions include discussion of a supergene vein-forming Ni-silicate mineral, garnierite.

FIELD AND LABORATORY METHODS

In each geochemical profile we sampled the soil, saprolite (in place soft weathering products); weathered, relatively fresh joint blocks (corestones), and unaltered, ultramafic bedrock where possible. Samples of known volume (about 309 cubic centimeters) of soil and saprolite were obtained using a hand percussion piston coring device. Samples too hard for this method were taken intact and returned to the laboratory. Bulk density measurements were made on these samples after drying by weighing and coating them with molten paraffin wax followed by immersion in water to measure their displaced volume. Bulk densities were determined by mass per unit volume with errors of about 0.5 to 1.0 percent. Average mineral grain densities were determined using an A.S.T.M. method by grinding samples to less than 200 mesh, boiling them to expell air bubbles, and determining volume accurately in a 1000 cc volumetric flask. Rock chemistry is discussed later. All data are presented in Appendices 1 (Eight Dollar Mountain) and 2 (Nickel Mountain).

ULTRAMAFIC PROTORES

Eight Dollar Mountain, Oregon

A harzburgite (chromite orthopyroxene-bearing olivine ultramafic) protolith has been weathered to a thin, 1 to 3 meter thick laterite on the top and flanks of a rounded mountain in the Josephine Peridotite of southern Oregon. The protolith harzburgite (sample 1100-44 in Appendix 1) contains 0.24 weight percent nickel and has a bulk density of 2.95 grams per cubic centimeter. Its grain density is 3.10 and porosity is 0.05, or 5 percent. In all, four soil profiles were sampled in exposures existing as the walls of exploration trenches at Eight Dollar Mountain. All four profiles are essentially similar in terms of nickel concentration and density changes. In general, with increasing depth nickel enrichment factors vary from about 2.5 for pelletal (pisolitic) soils to a maximum of 3.5 at a depth of 2 meters, returning to a value near 1.0 at about 3 meters depth. Density ratios (ρ_p/ρ_w) increase from 2.5 gram per cc in soils to a maximum of about 3.5 at 2 meters, and return to 1 at 3 meters depth. All values are shown and identified by sample number in the following figures and presented numerically in Appendix 1.

Compilation of all of our data on the four trenches at the Eight Dollar Mountain site shows a clear linear trend of increasing nickel enrichment factor with increasing density ratio of protore to weathered material (Fig. 3). This data array plots directly over the simple closed chemical system mass balance model calculated from Eqn. (6) for residual nickel enrichment for the case when the net deformation is zero, (that is, the strain term $\epsilon_{i,w}$ is equal to a value of zero) indicating that simple residual weathering occurred. Besides very little, if any, deformation of a systematic nature, it is clear that little if any supergene enrichment occurred.

The weathering path shown as open arrows in Fig. 3 indicates that protore harzburgite weathers through loss of mass from fresh hard rock through a corestone stage to, ultimately, soft saprolites. However, the data for soil plot differently than would be expected from a purely residual weathering profile, since one might expect soil to be simply the most weathered material. While the soil is less dense than the corestones, it is also more dense and less enriched in Ni than the saprolites on which it rests. The boundary between the soil and saprolite is abrupt, and the gravel size rocks in the soil are sometimes much less weathered than the saprolite immediately below. These observations indicate that the soil is derived from a mixture of upslope, less weathered materials exposed by mass-wasting processes and local weathering products; that is, it is colluvial.

The same data shown in Fig. 3 are plotted in Fig. 4 in terms of porosity. Porosity varies from essentially zero in the protolith harzburgite to over 75 percent in saprolites due to mineral dissolution and removal of elements other than nickel. Magnesium is the most

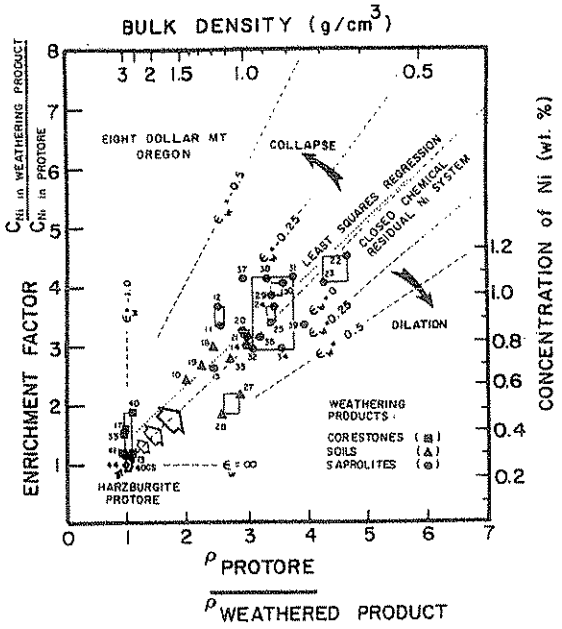

FIG. 3. Data array for the Eight Dollar Mountain deposit in the Josephine Peridotite ophiolite in southwestern Oregon. The boxes shown represent data for two samples (solid symbol) taken at the same depth in the weathering profile. The path of chemical weathering is from protore harzburgite (diamond symbol) to saprolite (circles), as shown by open arrows. Soils plot in intermediate positions because they develop on colluvium derived from landslides that expose relatively fresh peridotite-to-soil forming processes. Closed chemical system mass balance lines are shown for various amounts of deformation, either collapse or expansion. A least squares linear regression of all data gives a y-intercept of 0.434, a slope of 0.926, and a correlation coefficient of 0.86, producing a curve which is very close to the residual enrichment model y-intercept of 0.0 and slope of 1.0. Coincidence of the data array with the zero deformation curve implies that chemical weathering was dominated by residual enrichment of nickel and involved little, if any, strain. This is especially interesting as the bulk dry density of some saprolites is as low as 0.6 grams/cm^3, consistent with exceedingly high porosities due to mineral dissolution.

extensively leached. It is surprising that such extensive dissolution has occurred without collapse.

In Fig. 5 the Eight Dollar Mountain data are plotted in a bulk density and grain density graph contoured with lines of constant porosity. The data define a discontinuous, two-part weathering path that indicates the relative importance of mineralogical change (growth of low average grain density minerals, *e.g.*, serpentine) *versus* simple fracturing and mass loss with creation of higher porosity without significant mineralogical change. It is apparent that the initial weathering process is the change from protolith ultramafic rock to corestone. This represents primarily a small mineralogical change, that is, minor fracture-controlled serpentinization with negligible change in porosity. In contrast, the segment of the path over which corestones are converted to saprolites occurs through an abrupt change to lower bulk sample densities and higher porosities.

The gap in our samples is real and results from the simple fact that saprolites are porous and are rendered soft enough by weathering to be effectively penetrated by a piston coring device. The abrupt interface between saprolite and the edge of a corestone is shown in a field exposure (Fig. 6) where surface relief of the hard corestones is obvious. In Fig. 5 the much softer saprolite spanning a wide range in grain densities reflects the complex but systematic mineralogical alteration effects common to laterites.

The relative vertical position of minerals in laterite profiles have been well studied and have been shown by GOLIGHTLY (1981) to be largely controlled by the relative incongruent aqueous solubilities of minerals from the least soluble, *e.g.* goethite, occurring at the top, through Mg- and Ni-talc and serpentine with intermediate solubilities, and finally to the most soluble, such as pyroxene and olivine, at the bottom of the profile.

Nickel Mountain, Oregon

Two protoliths are exposed in the open pit mine at Nickel Mountain: one a light green peridotite (samples 1100-1A, B, C), and the other a much darker dunite (samples 1100-2A, B, C) (see Appendix 2). The fresh peridotite contains 0.23 percent nickel and has a bulk density, grain density, and porosity of 2.92, 3.00, and 0.01 respectively, based upon measurements of three large-volume samples. The fresh dunite contains 0.32

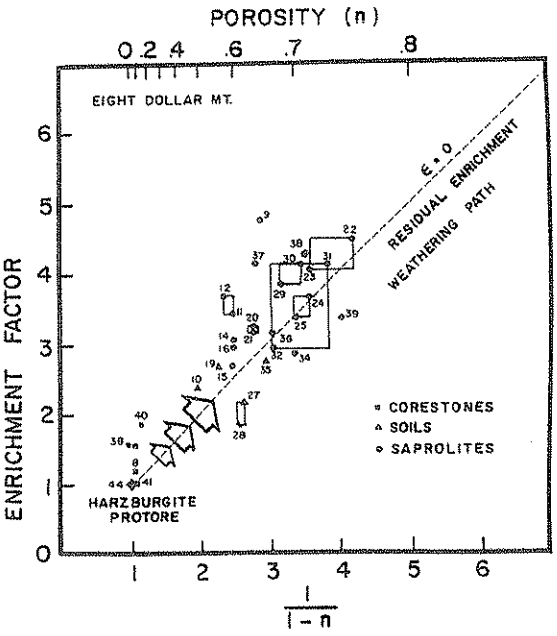

FIG. 4. Enrichment factor for nickel as a function of porosity using data from the Eight Dollar Mountain Prospect, Oregon. Boxes connect samples taken at the same depth.

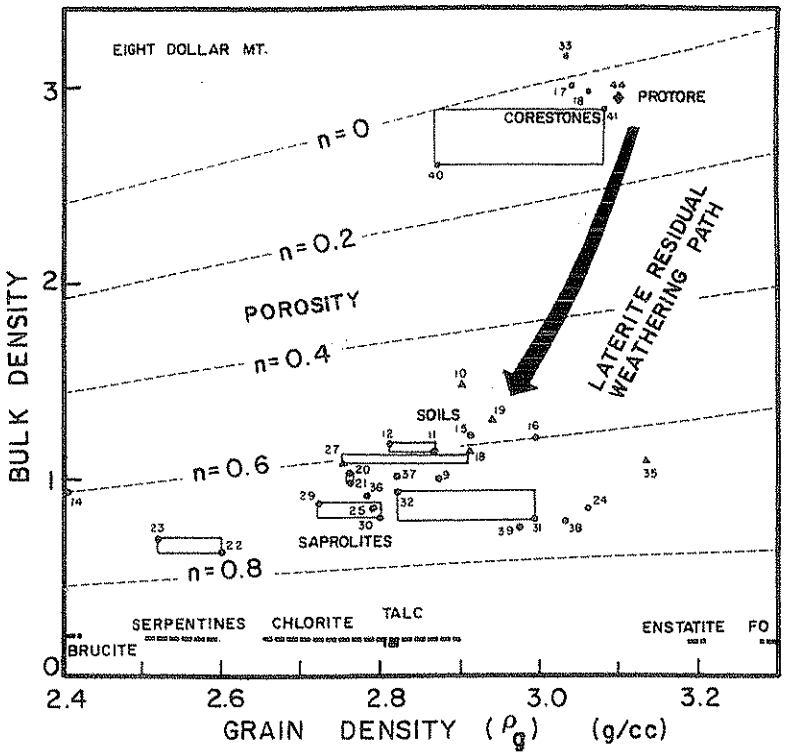

FIG. 5. Variation in bulk density as a function of average grain density and porosity from the Eight Dollar Mountain Prospect. Laterite residual weathering path is indicated with a solid arrow extending from the harzburgite protolith, corestones, soils, and saprolites as porosity increases from essentially zero to over 70 percent. Typical grain densities of minerals are shown.

percent nickel and has a bulk density, grain density, and porosity of 2.92, 2.90, and 0.007, respectively.

As at Eight Dollar Mountain, nickel enrichment factor profiles are similar in the four sites studied and increase in value from about 3 in pisolitic red soils to between 2 to 7 at a depth of 2 meters, attaining a value between 1 and 2 below 4 meters. Similarly, the density ratio of protore to weathered material increases from a value of about 3 in the soils to 3.5 at 2 meters, and attaining a value of 1 below 3.5 meters. The data from four soil profiles from Nickel Mountain are summarized in Fig. 7 using the density ratio as the independent variable. It is clear from the position of the data in relation to the residual enrichment line that in addition to the residual enrichment path shown by open arrows, there is a well-developed supergene enrichment trend (Eqn. 9) indicated by solid arrows emanating from peridotite protore values of density and nickel concentration at a slope initially much steeper than that of the residual path. This conclusion is based upon the much steeper slope for corestones than those saprolite samples which show a simple residual enrichment trend. Were this steep slope for enrichment of corestones due instead to residual enrichment, several hundred percent collapse would be indicated. However, this possibility can be ruled out as parts of these same profiles between joint structures have saprolite data arrays indicative of simple undeformed residual enrichment. Also, field inspection gave no indication of collapse.

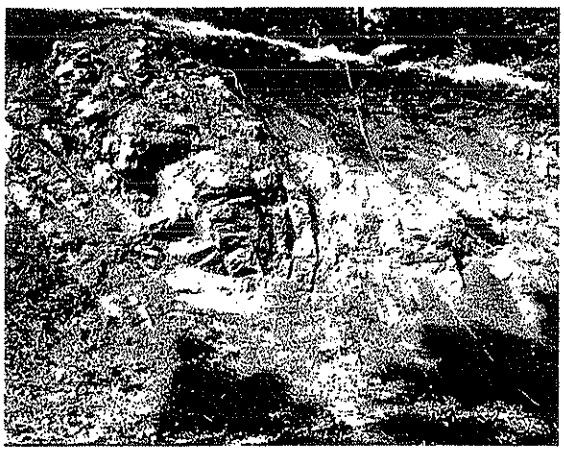

FIG. 6. Field photograph of the trench wall at Eight Dollar Mountain site number 2. Relatively unaltered corestones comprise the resistant unit on the left. Saprolites are much softer and are sampled using a piston coring device. Vertical dimension is about 4 meters.

Our result supports earlier speculations about the importance of supergene processes in providing ore grade nickel concentrations at Nickel Mountain (CUMBERLIDGE and CHASE, 1968). Previously, super-

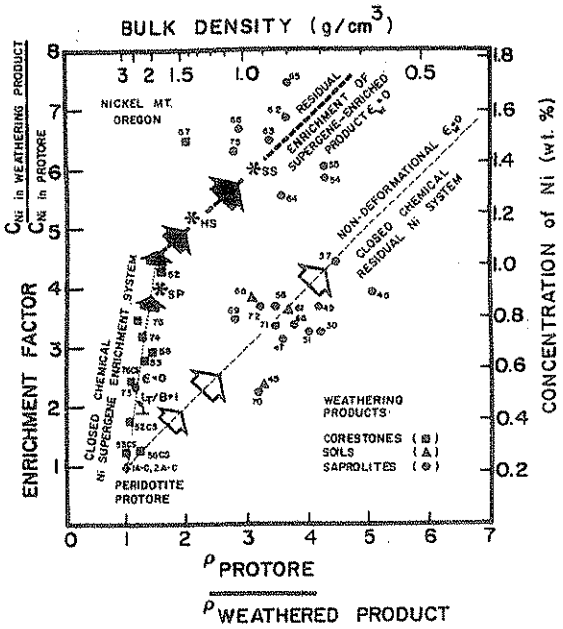

FIG. 7. Data array for the Nickel Mountain Mine area, southwestern Oregon. In addition to a residual enrichment path of chemical weathering (open arrows) extending from protore (diamond), strong supergene effects are evident, producing Ni contents as much as twice as high as those obtained at Eight Dollar Mountain 80 km to the north. The decrease in slope of the supergene array is probably due to residual enrichment of corestones previously enriched by supergene transport, resulting in a segmented weathering path (solid arrows). The slope of the initial supergene weathering path is given by $L_{T_{ip}}/B_{j,p} + 1$, which is the thickness ratio of the zone of nickel leaching to the zone of enrichment, plus 1. The subsequent, flatter slope is much less well-constrained and is shown as being 1, that is, non-deformational residual enrichment. Samples depicted by asterisks (SP, HS, and SS) represent saprolitized peridotite, hard saprolite, and soft saprolite, respectively, and are calculated from assay and dry, *in situ* tonnage factor (density) data published on the Upper Ore Body at Nickel Mountain (CUMBERLIDGE and CHASE, 1968). These represent 200 ton bulk samples of much larger volume than other data points which are for samples taken with small, 206 cm^3 piston cores and demonstrate that both sampling methods give compatible results. CS are cored centers of core stones. These are taken to sample the least altered centers of core stones.

gene effects were inferred simply from the vein occurrence of the green nickel-silicate garnierite. This evidence alone, while important, provides no indication of the relative contributions of residual and supergene enrichment. Analysis of individual profiles reveals that in some instances, both types of weathering have occurred. Near the main ore body at Nickel Mountain, supergene effects seem to dominate and are responsible for enrichments of up to eight or nine times protore values. Parts of the saprolite and corestones alike are enriched by supergene processes. Nickel enrichment of core stones (Figs. 3 and 7) may be due to several factors including the proximity of the corestone rinds to fluids moving through permeable fracture, adsorption of Ni by Fe-rich rinds, or lateral movement of Ni-rich fluids. Near the edge of the ore deposit, however, supergene enrichment is not as pervasive, being more localized in reddish colored joint and fault fillings and within corestone samples at depth (Fig. 8).

While profiles studied to date indicate that both residual and supergene enrichment have occurred at Nickel Mountain, we have not recognized any indication of the zone leached in Ni which must have overlain the main laterite enriched in nickel. In all likelihood, the upper part of the deposit has been taken away both by natural erosional processes and through mining, removing all evidence of the leached zone.

Summarizing our lateritic studies, mass balance analysis of lateritic profiles provides clear evidence of the nature and extent of the ground water transport processes and offers a means of discriminating between the effects of residual and supergene weathering processes. Supergene enrichment is shown to be necessary to affect sufficient concentration of nickel to warrant economical mining as at Nickel Mountain. This may be the primary difference between mineable deposits and hundreds of laterites formed simply by residual enrichment of ultramafic rocks.

PODZOLS

Application of mass balance models to podzols sampled along the Pacific coast several kilometers inland from the town of Mendocino, California, within the Jug Handle Reserve provide an opportunity to study both residual and supergene enrichment processes. These soils in the Pygmy Forest, developed on

FIG. 8. Field photograph of a highly jointed laterite exposure at Nickel Mountain, Oregon, site number 4. Reddish pelletal (pisolitic) soil overlies joint corestones and saprolite. Supergene transport is controlled by joints.

beach sands overlying wave cut platforms in graywacke bedrock. The soils have been the subject of intensive study by soil chemists and ecologists (JENNY *et al.*, 1969; JENNY, 1980) working on chronosequence and ecosystem evolution. A set of five marine terraces, each progressively older with increasing distance from the coast, were formed during intervals of sea level rise. Each has undergone weathering of essentially the same type of protolith beach sand under similar climatic and topographic conditions as sea level dropped and the terraces became elevated. The first terrace is at 30 meters, with the other older terraces at 58, 100, 140, and 217 meters above present sea level. We present here an analysis of soil profiles sampled on the fourth terrace. Our samples of protolith (11-7-28, 29, 30 in Appendix 3) come from Terrace 1, and consist of unconsolidated beach sands within 50 meters of the ocean. These samples are used as reference materials and are depicted in the subsequent podzol profiles (Figs. 9–11).

The podzol soil profile we have studied in detail is exposed in a trench. Our description is summarized in Fig. 9 using the horizon designations of BUOL *et al.* (1980). The profile is separated into albic and spodic zones. The uppermost horizon is a densely rooted, organic-rich A1 soil. Beneath this zone is a white E, or eluviated horizon. This is underlain by a purplish A3.

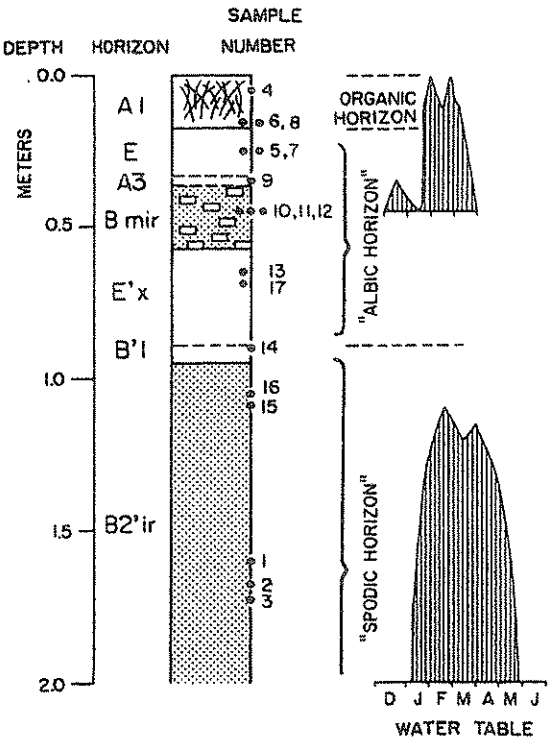

FIG. 9. Soil profile description of podzol exposure in the Pygmy Forest of the Mendocino coast, California. The position of ground water table is from JENNY *et al.* (1969). Notice that in addition to the main ground water table which ascends during the wet season to a depth of close to one meter, there is a perched water table directly above a zone of low porosity (Fig. 10). Metal enrichment is confined to these saturated zones.

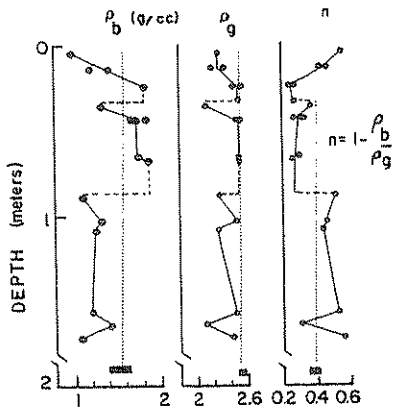

FIG. 10. Depth profile of physical properties of a podzol on Terrace 4 of the Jughandle Reserve, Mendocino County, California. Values of supposed protolith material are shown as solid bars which represent the range of three samples. The average is shown with a dotted line. These are from Terrace 1 beach sand deposits (1107-28, 29, 30 and Appendix 3).

The underlying Bmir horizon is buff colored, with thin red bands and hard pan development. A second E horizon, white with red bands, occurs beneath the Bmir. It is dense and brittle, suggesting fragipan development (E'x). A transitional, B'1 horizon, mottled grey and purple, lies over a stiff, reddish-brown B2'ir horizon. The typical unweathered C was not observed. Also shown in Fig. 9 is the position of the ground water table (JENNY *et al.*, 1969). In the wet months, it ascends to a depth of about 1 meter. Above the main ground water table during the wet months a perched ground water table forms directly above the impermeable hardpan of the Bmir layer. We will show that this hydrologic regime is clearly related to the geochemistry and metal transport behavior of the podzol.

Figure 10 shows our data on the physical properties from the surface to a depth of two meters. Three samples of sand from Terrace 1 (nearest the coast) are included to give an indication of the values of bulk density, grain density, and porosity of the least altered or protolith material. The uppermost horizon, the A1, dominated by organic compounds and roots, exhibits a bulk density increase from very low values at the surface to a depth of about 0.2 meters. Porosity of the organic-rich layer decreases to this same depth. From 0.2 to 0.9 meters bulk density is relatively high due to the low porosity values as average grain density varies only a small amount. Explanation of this intermediate set of soil horizons with high bulk density and low porosity is essential to understanding these podzols. Below 0.9 meters, bulk density is slightly lower and porosity is higher than corresponding values of protolith beach sand from Terrace 1 (dotted line). These effects are discussed in terms of related changes in chemical composition.

The chemical profiles corresponding to that of physical properties (Fig. 10) are given in Figs. 11A–E. At a depth of approximately 0.9 meters abrupt changes in composition occur. We will use the nomenclature of soil chemistry for soils (BUURMAN, 1984) above this

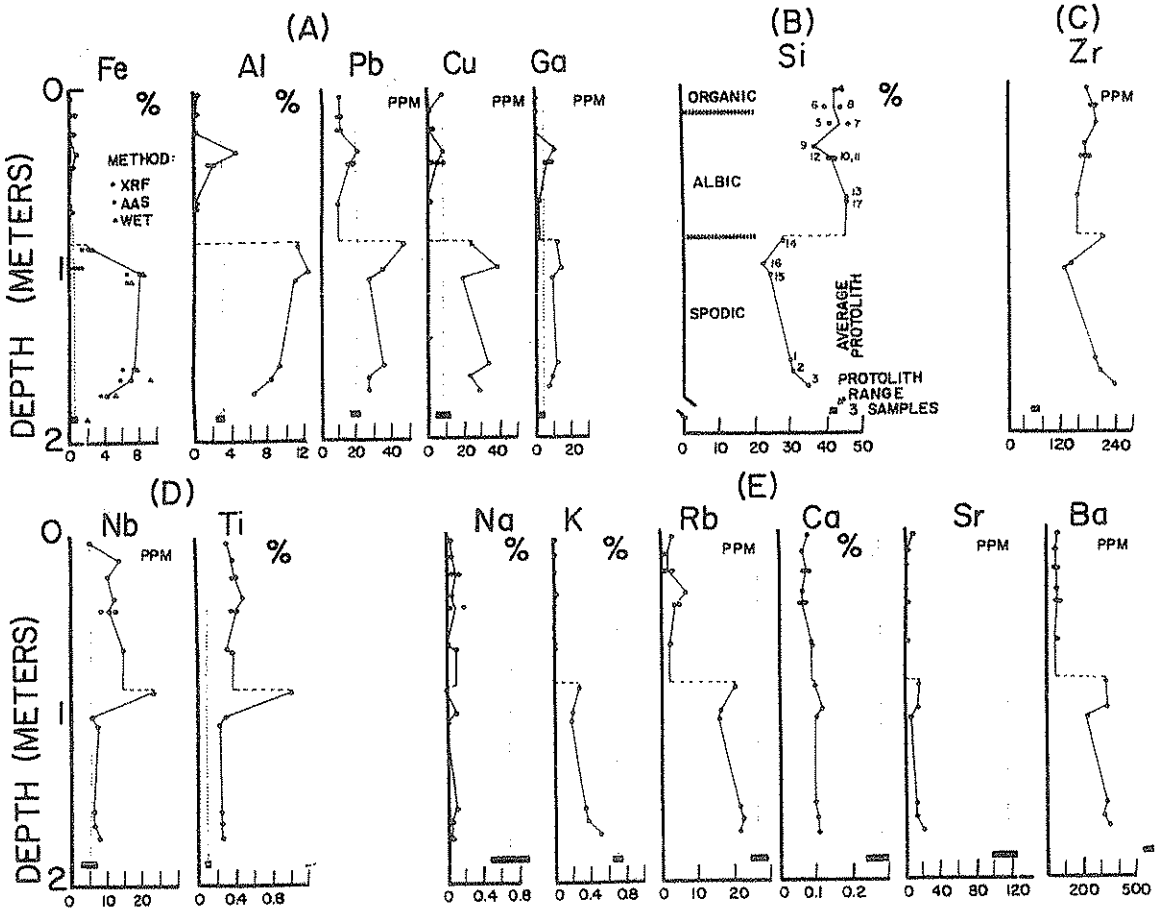

FIG. 11. Chemical profiles for the same samples represented in Fig. 10. All analyses were done by XRF unless noted otherwise, as in (11A), where Fe analysis has been performed also by AAS and wet chemistry for comparison. Al and Si have also been analyzed by wet chemistry to check accuracy of XRF techniques. XRF results are accurate to about 5 percent of the amount present. (11A) Fe, Al, Ga, Cu, and Pb are all leached in the albic zone and are reprecipitated in the spodic zone. Compare the position of these enriched zones with the depth of the ground water tables during the wet season (Fig. 9). Dotted lines are the average of three protolith samples. Their range is given by a solid bar. (11B) Silica appears to be slightly enriched in the albic zone, implying quartz stability. This is not the case, as discussed in the text, and instead results from the more complete dissolution of other, less abundant elements such as Fe and Al. (11C) Zr appears to have little systematic variation. (11D) Nb and Ti are residually enriched in the albic zone with rutile, TiO_2 as the host mineral.

transition (albic) and those below (spodic). It has been recognized that many albic horizons have been leached of Fe and Al which have been transported downwards and enriched in the underlying spodic zone. Typically the spodic zone is also enriched in organics, but these are not so at the site studied. In Fig. 11A we see the expected leaching of Fe and Al in the albic zone but we have also discovered that Ga, Cu, and Pb are leached, with enrichment of all these elements below this depth down to 2 meters, where protolith concentrations are approached. These elements have been transported by supergene processes. The profile for Si is shown in Fig. 11B, indicating slight enrichment in the albic zone and leaching from the spodic. Zr shows no systematic variation with respect to protolith concentrations (Fig. 11C). Figure 11D shows that Nb and Ti are enriched in the albic zone, from which Fe and Al have been leached. Finally, in Fig. 11E, we show that all alkali metals, K, Na, Rb, Ca, Sr, and Ba are strongly leached from the albic zone, and in some cases are even leached from the spodic zone. Notice that within the albic zone proper there is a thin zone enriched in Al, Fe, Pb, Cu, Ga, and Rb which is depleted in Si above the main zone of enrichment composing the spodic zone.

The nature of the secondary precipitates containing Fe and Al in the spodic as well as the upper thin zone in the albic horizon is illustrated in Fig. 12. This is a transmitted light photomicrograph of impregnated plus 20 mesh particles in the upper supergene enriched zone. Large clasts of quartz cemented by an aggregate of minute quartz grains and a matrix material containing the Fe, Al, and Si, determined using the electron microprobe, are typical. The angularity of the fine-grained quartz in the dark matrix may in part be due to physical breaking of grains along fractures. The zones of enrichment of Fe and Al are the only intervals in which plus 20 mesh particles occur. The secondary Fe, Al,

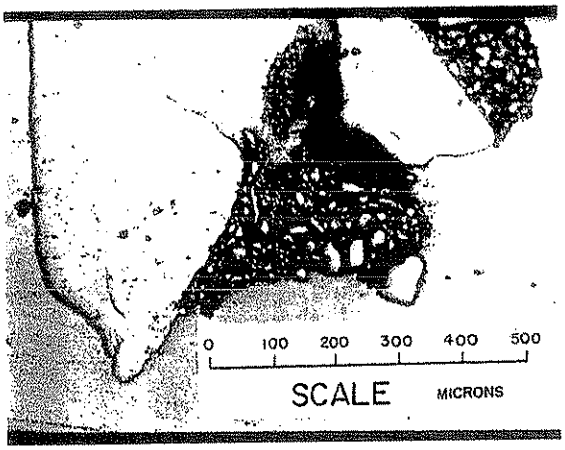

FIG. 12. Reflected light photomicrograph of sample 1107-11 grain concentrate with specific gravity less than 2.96, greater than 20 mesh. Matrix material is composed of transported and enriched Fe, Si, and Al precipitates cementing fine-grained quartz. This is the Bmir soil horizon shown in Fig. 9 (left) and corresponds to the upper perched enrichment zone indicated in Fig. 11. It corresponds to the perched ground water table of Fig. 9 (right).

and Si precipitates are invariably white in color and are easily separated from bulk samples using a 20 mesh screen. This is a practical field method for identifying zones of even the slightest enrichment as the upper or perched enrichment zone contains these grain aggregates (samples 1107-9 through 1107-12 and Fig. 12).

The correlation of the wet season saturated zones with the upper and lower zones of Fe, Al, Ga, Pb, and Cu enrichment is not simply coincidental and indicates a clear hydrological-geochemical link on the leaching and enrichment processes. Two observations are relevant to explaining this correlation. First, significant moisture is necessary to produce the organic acids which act as chelating agents to transport metals. Second, saturated conditions must somehow be necessary for fixation of these supergene metals. The sharp division between the leached and enriched subsystems is probably the interface between saturated and unsaturated conditions during the wet season. This interface has been shown in Cu supergene systems to control the oxidative release of metals by acid attack from pyrite oxidation in the presence of oxygenated ground gasses (BRIMHALL *et al.*, 1985). These soluble species are carried downward by unsaturated flow and reprecipitated as sulfides by neutralization reactions utilizing available sulfide sulfur occurring as pyrite in the zone of saturation, either within the capillary fringe or below the ground water table. This secondary reprecipitation occurs largely because of major reductions in the oxidation potential as oxygen-rich gases are no longer present. Minerals such as magnetite, biotite, and alkali feldspar in the unoxidized protolith buffer oxygen fugacity at values orders of magnitudes lower than in the unsaturated zone. The occurrence of a perched water table presents two opportunities for this oxidation-reduction transport and fixation of metals. Such perched enrichment zones are not uncommon in supergene Cu systems.

Because of the coincidence of the saturated zones (Fig. 9) in the wet season and the two enriched zones of the podzols, it is fairly certain that the hydrochemical fractionation patterns measured here are part of a transport process which is operative today, although the soil horizon development to the present state must have contributed to the progressive modification of the hydrologic process (JENNY *et al.*, 1969). The study of such contemporary processes presents unique opportunities for expanding the present understanding of transition metal geochemistry and for measuring relevant fluid flow velocities, hydraulic conductivities, permeabilities, and hydraulic gradients as well as for sampling fluids.

The metasomatic effects in the albic and spodic zones can be evaluated beyond this descriptive level by using the compositional data in conjunction with the mass balance relationships involving density, zonal volume, porosity, and strain. In Fig. 13A we show the behavior of Al, a clearly supergene element compared with that of Nb (Fig. 13B) which is one that we show is immobile. The former has been redistributed from the leached albic zone down into the enriched spodic zone, as has been the case also with Fe. Nb, in contrast, is more abundant in the albic zone than in the protolith and occurs with essentially protolith concentrations in the underlying spodic zone. The lack of evidence to suggest coupled depletion and enrichment of Nb as there is for elements having undergone supergene transport processes indicates that the Nb pattern may result from residual enrichment. Were there no deformation in the albic zone, Nb data would plot simply along a linear path as in the spodic zone. This is clearly not the case; the only alternative is to invoke deformation, specifically, collapse in the albic zone, to explain the Nb pattern. This is quantified, solving Eqn. (8) for strain ϵ yielding

$$\epsilon_{i,w} = \frac{C_{i,p}}{C_{i,w}} \frac{\rho_p}{\rho_g} \frac{1}{1-n} - 1. \qquad (11)$$

The results of this calculation of strain using a combination of chemical, bulk density, grain density, and volumetric data, is shown in Fig. 14A for Nb and in Fig. 14B for Ti. The calculation for both elements indicates 60 percent collapse. The root zone has a net positive strain of about 70 percent based on Nb, which is probably the result of root growth dilation.

Inspection of heavy mineral separates supports our conclusion that both Nb and Ti have behaved as immobile elements throughout the weathering column. Rutile, a very likely host mineral, has been identified as a ubiquitous phase throughout the column. While the rutile grains are rounded, their surfaces do not appear to be etched. Sphene, another possible Ti-Nb host, has not been found in the albic zone. Rounded euhedral zircon which is also ubiquitous, has surfaces which are

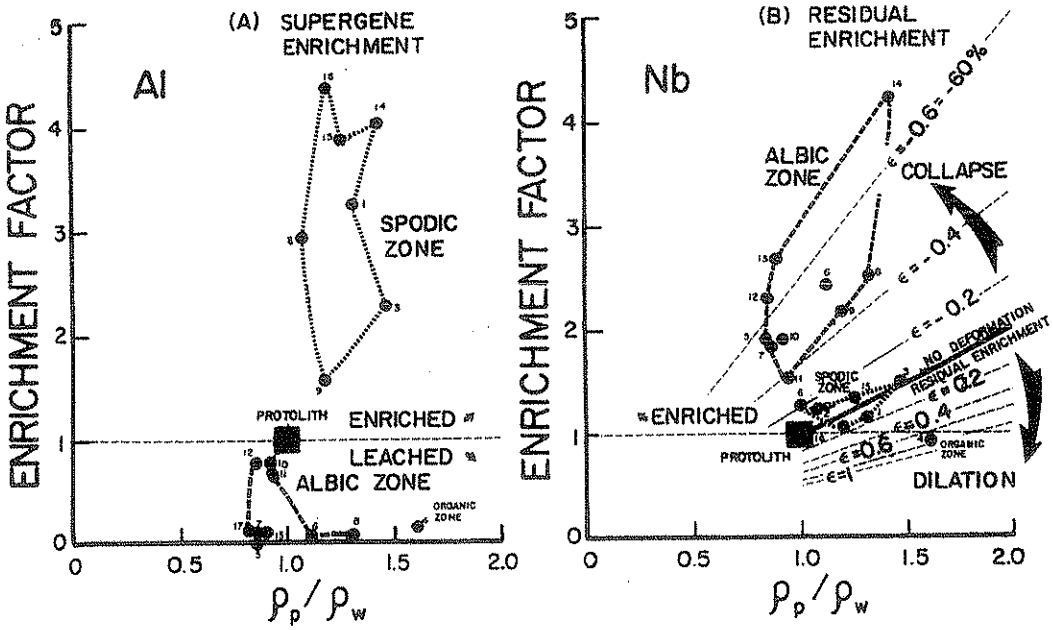

FIG. 13. Comparison of the fractionation factors of Al and Nb which are supergene and residually enriched elements, respectively. Closed system mass balance strain contours are shown from which Nb enrichments may be interpreted. Such analysis indicates strong dilational effects in the root and organic-rich zone and collapse in the albic horizon. Enrichment of Nb must be residual, as ground water flow is from the albic to the spodic. Depth of samples is indicated in Fig. 11C. Note sample 9 is from a perched enriched zone within the albic zone. Sample 14 is enriched in Fe and Al and is part of the spodic zone, but has strong residual Nb enrichment consistent with large amounts of collapse.

highly etched, implying that it has been partially dissolved. This is consistent with the lack of clear residual enrichment of Zr in the albic zone. Other heavy minerals identified throughout the profile include tourmaline and garnet. An alternative explanation is that aeolian additions to the albic zone have enriched it in Ti and Nb-bearing minerals. While possible, this interpretation seems less likely than the former collapse hypothesis.

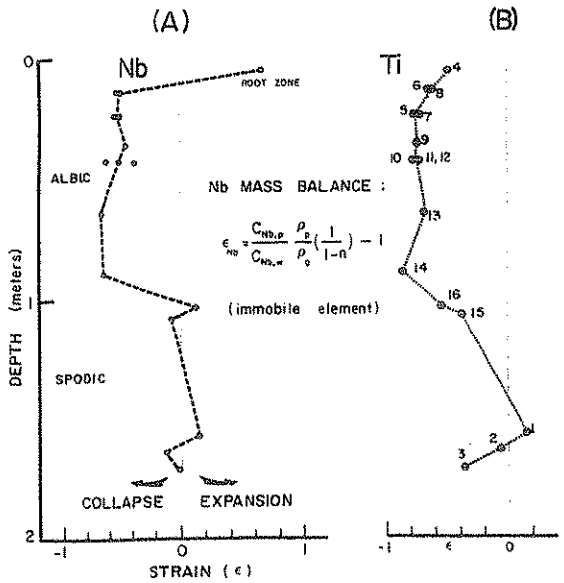

FIG. 14. Net strain profiles calculated using Nb and Ti enrichment factors. Both elements are contained in rutile. Sample 14 is a transitional horizon (see Fig. 9) for soil classification.

We propose, then, that the calculated 60 percent compaction of the albic zone which is born out by rutile stability has resulted from dissolutional collapse of the sandy material by organic acids. This much dissolution would result in significant reduction in the grain sizes present. We have tested this hypothesis through a grain size analysis of all samples. Results for the size ranges found in the protolith, albic, and spodic zones are shown in Fig. 15. Here it is clear that all samples of the albic zone contain considerably finer grains than the spodic, where our strain calculations imply no measurable collapse but simply the creation of fines through normal pedogenesis.

An estimate of the amount of dissolution necessary to produce this grain size change can be made from the mean grain sizes of the cumulative size curves of Fig. 15. Assuming spherically shaped grains, the reduction in mean grain size from 300 microns to 220 microns can be expressed in terms of the mass ratio of the present average weathered grains of 5.6×10^6 cubic microns to that of the original grains with 1.4×10^7 cubic microns, or a ratio of 0.40. This mass ratio is equivalent to a mass dissolution of 60 percent of the grains originally present in the protolith.

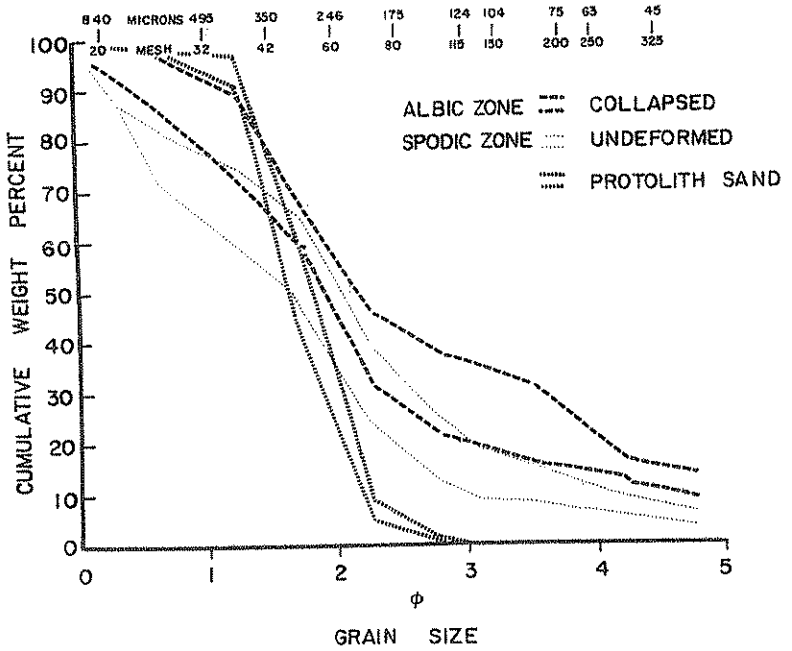

FIG. 15. Cumulative size frequency data showing the pedogenic fine fractions of the albic zone which is consistent with dissolutional collapse of the upper weathering zone.

Mass loss equation

This surprising conclusion is confirmed by using a form of Eqn. (8) derived in terms of mass ratios (Eqn. (12)) where the superscript zeros refer to the properties of the original protolith.

$$\epsilon_{i,w} = \underset{(1)}{\frac{\rho_g^0}{\rho_g}} \underset{(2)}{\frac{m_g}{m_g^0}} \underset{(3)}{\frac{1-n^0}{1-n}} - 1 \qquad (12)$$

The total mass of mineral grains in a representative elementary volume is given by m_g now and m_g^0 in the original protolith. In Eqn. (12), term 1, a grain density ratio has essentially a mineralogical effect which in the podzols is quite minor, having a value of 1.05, since the mean grain density in the albic zone is 2.39 in contrast to the original protolith grain density of 2.5 grams per cc. Term 2 is the mass ratio of interest in evaluating the hypothesis of dissolutional collapse. If term 1 is essentially equal to one, then term 2 may be viewed as a slope term of a linear curve expressing strain as a function of change in porosity, and term 3 varies from an initial value involving n^0 to a present value of n. In Fig. 16 we use Eqn. (12) to evaluate the hypothesis of dissolutional collapse of podzols. It is clear that the estimated amount of dissolutional loss of mass of about 60 percent from the albic zone is born out from an analysis of this figure in which between 40 and 70 percent loss of mass is indicated with an average of approximately 50 to 60 percent. The collapse mechanism is proven, and unquestionably is a dissolution of protolith minerals, predominantly quartz in the albic zone. Also apparent in Fig. 16 is an interesting lack of strain in the spodic zone, although between 5 and 35 percent mass loss has apparently occurred. This difference between the apparent mechanical behavior of albic and spodic zones implies that a certain amount of dissolution may occur without initiation of collapse.

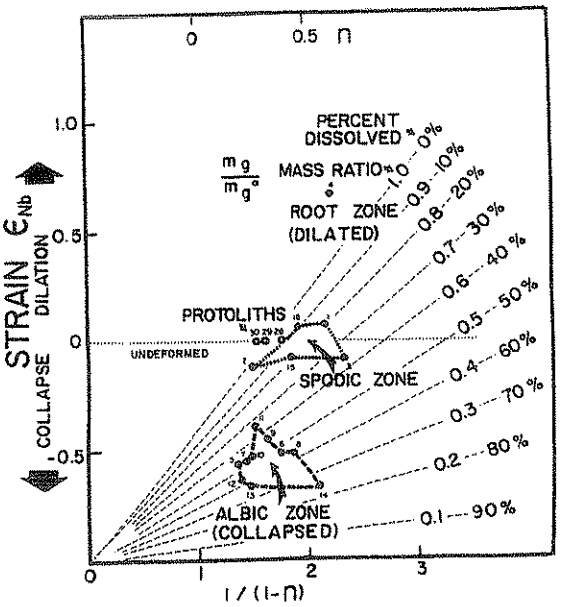

FIG. 16. Physiochemical-chemical strain (ϵ_{Nb}) as a function of porosity and percent mass dissolution. Protoliths are shown along the zero strain line. Root zone data implies dilation (positive strain). Spodic zone samples are undeformed but have experienced between 5 and 35 percent dissolution. Albic zone samples are collapsed and extensively dissolved between 40 and 75 percent by weight.

However, as mass dissolution approaches about 35 percent, collapse occurs.

For the sake of comparison, mass loss calculations have been done for the Eight Dollar Mountain laterite where no deformation has been found with our method, and major differences exist between the initial porosity of the protoliths: ultramafic rocks *versus* beach sands. Using appropriate values ($n^0 = 0.05$) indicates that corestones have undergone between 0 and 12 percent mass loss; soils between 50 and 64 percent, and saprolites between 50 and 64 percent. This dissolution has taken place without measurable strain, probably because of the strength of the ultramafic rock, in contrast to the loosely consolidated beach sand protolith of the podzols.

Separation of Si from Fe and Al in podzols

Explanations of the separation of Si from Al and Fe have commonly stressed the low solubility of quartz as the major factor in producing the albic horizon (CHESWORTH and MACIAS-VASQUEZ, 1985; COEN and ARNOLD, 1972), as quartz is the predominant mineral skeletal phase. The solubility of minerals such as allophane, imogolite, kaolinite, goethite, and ferrihydrite are thought to control Al and Fe solubility. Our results indicating dissolutional collapse of the podzol weathering column raise some serious questions about the prevalent view that the albic zone is due simply to leaching of Al and Fe, leaving quartz essentially unaffected. Instead, we have found that besides minerals containing the latter two elements Fe and Al, that Si as well has been leached extensively, but since quartz occurs as a more abundant species in the protolith, it was relatively enriched, as Fe and Al were almost completely depleted. This conclusion is consistent with measured natural water compositions in podzols samples in lysimeters (UGOLINI *et al.*, 1977), which show Si to have had the largest elemental loss from podzolic systems. We conclude that the residual enrichment of Si is simply the result of the other elements having been leached out more thoroughly. The stark white color of the albic zone has then, in effect, wrongly focussed attention on the retention of quartz and the loss of Fe- and Al-bearing minerals when, in fact, quartz too has been extensively leached with dramatic deformational defects.

PHYSIO-CHEMICAL STRAINOMETER

The constitutive equations derived herein provide a means of determining the amount of net strain in samples affected by reactive aqueous fluids. These developments eliminate the need for use of qualitative field estimates of strain using visual methods.

While application of our constitutive equations to podzols and laterites shows the utility of the methods, a precautionary note is offered to assure the correct use in future applications. An example is offered to avoid potential difficulties. As is well known, the nearly pure silica compositions in the albic zone which are responsible for the "ashen" white color of the horizon are caused by very strong organic acids leaching essentially every major mineral, including quartz. As quartz is the predominant mineral in our beach sands, the enrichment of SiO_2 (Fig. 11B) occurs by the more complete removal of other minerals. The SiO_2 enrichment is limited to a maximum value of 1.13, which is the ratio of 100 percent for a horizon consisting of pure quartz to the protolith concentration of SiO_2 of 88 percent. In contrast, trace elements like Nb can be enriched by large factors and used effectively to measure accumulated strain. A major constituent such as SiO_2 cannot, as it can only increase in abundance up to the point when it is the only major constituent present as all other major and minor phases are leached away in the albic zone. SiO_2 is not, therefore, a good species with which to determine strain. Furthermore, it is necessary, and possible with constitutive relations, to demonstrate that an element used for strain calculation has been immobile and, in this example, Si has not been so.

Besides the ground water table having an effect on dissolution and precipitation reactions, changes in permeability may control solution residence times. Near the top of the spodic horizon, permeability is much less than in the albic zone. This may be a "reaction" zone.

Interpretation of the immobile trace element strainometer

While Eqn. (11) gives the means of computing strain in metasomatic systems from the combination of chemical and physical properties, an intuitive rationale can be easily demonstrated from the definition of strain, that is, the change in volume divided by the original volume:

$$\epsilon_w = \frac{V_w - V_p}{V_p} = \frac{\dfrac{m_g}{\rho_g(1-n)} - \dfrac{m_g^0}{\rho_g^0(1-n^0)}}{\dfrac{m_g^0}{\rho_g^0(1-n^0)}}. \qquad (13)$$

Here, the superscripted zeros refer to the initial protolith states; the remaining terms referring to the present weathered products. Note here that we are not concerned with the concentration of any specific trace element, but simply the overall volume change. In practice, we use Eqn. (11) to determine strain, since the mass terms given in Eqn. (13) are difficult to evaluate but serve well for purposes of illustration. Strain ϵ_w, either positive or negative, results from a significant difference between the weathered system volume V_T and that of the original representative elementary volume V_{T^0}. It is seen that each volume term has three parts: total mineral grain mass, average grain density, and porosity. These three factors are related in a quotient which reduces to

$$\epsilon_w = \frac{m_g \rho_g^0 (1-n^0)}{m_g^0 \rho_g (1-n)} - 1. \qquad (14)$$

In order for a representative elementary volume to remain unchanged and unstrained, the quotient must be equal to one, in which case there must be compensating effects between the factors. If there is mineral dissolution (m_g decrease), either the average grain density must decrease too or the porosity must increase to maintain the original volume. If cementation occurs and mineral mass increases, then porosity must obviously decrease unless the cement has a high average density. If alteration reactions produce low density grains, then there must be dissolution or porosity decrease.

Potential applications of the strainometer: Physio-chemical mechanics

Through this analysis emerges an acute awareness of the possible variety and complexity of heterogeneous metasomatic reactions between aqueous fluids, gases, and minerals in rocks and soils. It is clear that processes which are non-deformational would seem rather exceptional in nature, at least in granular materials, given the requirements of special compensating relationships indicated in Eqn. (14). The common assumption of volume-for-volume replacement of primary minerals by secondary assemblages should be questioned, as it may have in many instances been invoked simply for the sake of convenience and lack of a true understanding of the real strain history of hydrochemical systems. We now have a practical means to ascertain strain histories and to relate them rigorously to the strength and mechanical properties of the wide spectrum of earth materials which interact with reactive surficial fluids. The potential is enormous for such applications, including analysis of the effects of loading and compression of weathering columns, collapse by chemical dissolution and weakening of the grain matrix structure, and dilation by root growth. In basin analysis and diagenesis studies, use of empirical relationships expressing pore volume collapse, such as Athy's law which is based simply and solely on correlation of porosity with depth in sedimentary basins can be improved upon by performing actual strain calculations. Migration of metamorphic fluids and metamorphic processes should be fertile ground for development of knowledge of the hydro-mechanics of intermediate depth crustal processes. With the array of chemical-mechanical processes which could be illuminated from these applications, interrelationships between transport processes could be developed. Below we offer one such example relating surficial mechanical erosion to subsurface dissolutional collapse.

TABLE 1. Pygmy Forest podzol data for supergene elements and physical rock (soil) properties used in paleosurface reconstruction (Eqn. (15)). $L_{T_{j,c}}$ is the current thickness of leached zone for element j.

	B_p (m)	$C_{j,p}$	$C_{j,e}$	$C_{j,l}$	ρ_p (g/cc)	ρ_e (g/cc)	ρ_l (g/cc)	ϵ_e	ϵ_l	$L_{T_{j,c}}$ (m)
Fe	1.0	0.61%	6.6%	0.17%	1.55	1.23	1.61	0	-0.6	0.88
Al	1.01	2.85%	9.5%	0.47%	1.55	1.25	1.63	0	-0.6	0.83
Pb	1.05	19.0 ppm	32 ppm	11.0 ppm	1.55	1.25	1.63	0	-0.6	0.83
Cu	1.13	8.0 ppm	26 ppm	0.9 ppm	1.55	1.26	1.62	0	-0.6	0.75
Ga	1.13	3.6 ppm	16 ppm	1.1 ppm	1.55	1.26	1.62	0	-0.6	0.75

TABLE 2. Calculated results for the amount of leached protolith. $L_{T_{j,c}}$ is the calculated value using Eqn. (15). $L_{T_{j,c}}$ is the leached column height corrected for net strain, i.e., $(\epsilon + 1)^*L_{T_{j,c}}$. Surface erosion is given by $L_{T_{j,c}} - L_{T_{j,c}}$. The main point is that the average amount of subsurface erosion (2.0 meters) computed on the basis of dissolutional collapse indicated by Nb enrichment is three times that of surface erosion (0.65 meters) determined using excess supergene enriched metals (Fe, Al, Ga, Cu, and Pb) in the spodic zone. These quantities have been converted into average rates using an assumed terrace age of 400,000 years, which is consistent with age estimates and correlations on the Mendocino coast.

	$L_{T_{j,c}}$ (m)	$L_{T_{j,c}}$ (m)	Surface Erosion (m)	Rate of Surface Erosion Over 400,000 Years (mm/y)	Subsurface Erosion (m)	Rate of Subsurface Erosion Over 400,000 Years (mm/y)
Fe	8.7	3.5	2.6	0.0065	5.2	0.013
Al	1.9	0.75	0	0	1.1	0.0028
Pb	0.49	0.20	0	0	0.29	0.007
Cu	2.0	0.79	0.04	0.0001	1.18	0.0030
Ga	3.4	1.4	0.62	0.0015	2.06	0.0052
Average			0.65	0.0016	2.0	0.005

Paleotopography and surface versus subsurface erosion

Solving Eqn. (5) for the total leached column height $L_{T_{j,p}}$ yields the total leached column height before surficial erosion for each supergene element j:

$$L_{T_{j,p}} = \frac{B_{j,p}(C_{j,e}\rho_e(\epsilon_{i,e}+1) - C_{j,p}\rho_p)}{C_{j,p}\rho_p - C_{j,l}\rho_l(\epsilon_{i,l}+1)}. \qquad (15)$$

As developed in BRIMHALL *et al.* (1985), chemical and physical data can be effectively used to infer the paleotopography at the time of initiation of subsurface supergene chemical transport. We now apply these techniques to podzols and incorporate the deformational aspects of these hydrochemical systems.

Data used for Fe, Al, Cu, Ga, and Pb concentrations are given in Table 1. Substitution of field and laboratory data into Eqn. (15) yields independent estimates of the amount (vertical column height) of protolith beach sand which was leached of each element to yield the excess mass of the same elements in the enriched zone. Calculated results are given in Table 2. The average amount of surface erosion is calculated as 0.65 meters. This average may be somewhat high, and results using Fe are distinct from those of Al, Ga, Cu, and Pb. The amount of subsurface erosion, that is, landscape lowering due to chemical dissolution and collapse of the albic zone, a strain of minus 60 percent, averages about 2 meters, or about three times as much as that removed by surface transport. This is an exciting result which is consistent with the relatively flat surface of the terraces and the permeable nature of the sandy protolith in which infiltration rates must have been high, at least during the initial phases of weathering. For the podzols studied here we conclude, then, that chemical erosion through deformation must play an important and apparently uniform role in their landscape evolution.

BAUXITES: A PREDICTION

A classical problem of major interest which immediately emerges as being suitable to mass balance anal-

ysis is the formation of bauxites. These residual accumulations of Al-rich minerals in warm tropical regions form where it is thought that surface erosion is slow and the geomorphic processes are in a sufficiently dynamic state as to promote active leaching with only minor water table fluctuations (GRUBB, 1970). Though we do not have as yet sufficient field and laboratory data to offer a quantitative analysis of the amount of erosion, erosion rates, or deformation attending bauxitic weathering using our mass balance methods, we can possibly offer some insight into the formation of these important deposits and speculate further about their origin. These comments are offered, then, in part to stimulate further analytical field investigations which build upon the excellent published descriptions referenced below.

A large number of insightful observations have been made on bauxites, but the broad significance of bauxites in regards to interrelated hydrochemical, geomorphic, and sedimentological processes can be significantly expanded upon. Specifically, chemical enrichment patterns of Zr, Ti, and Cr have been published (SADLEIR and GILKES, 1976) which exceed factors of 3 to 4.5, indicating strong residual enrichment of these elements in stable mineral phases and, quite possibly, extreme levels of deformational collapse. This prediction is born out by the high levels of detrital heavy minerals which in many instances increase in abundance upwards in bauxitic weathering columns (GRUBB, 1970, 1971) in the Gove profiles of northern Australia. At the Gove and Weipa desposits in northeastern Australia (GRUBB, 1971) and the Jarrahdale bauxite deposits of the Darling Range in western Australia (SADLEIR and GILKES, 1976), rutile is a common mineral phase in the dense fraction, as is anatase, although the latter has been interpreted previously as being authigenic as a leucoxenisation product of ilmenite (GRUBB, 1970). We infer from the available data that significant collapse may have occurred during weathering over expansive areas of Australia and elsewhere where major bauxite deposits occur. We base our inferences on a combination of data which previously would have seemed unrelated for lack of constitutive relationships.

Furthermore, in light of the thickness of these deposits and the implications from our analytical methods, we infer from the geochemical profiles and heavy mineral distribution patterns in bauxite that tremendous but as yet unknown thicknesses of protoliths have

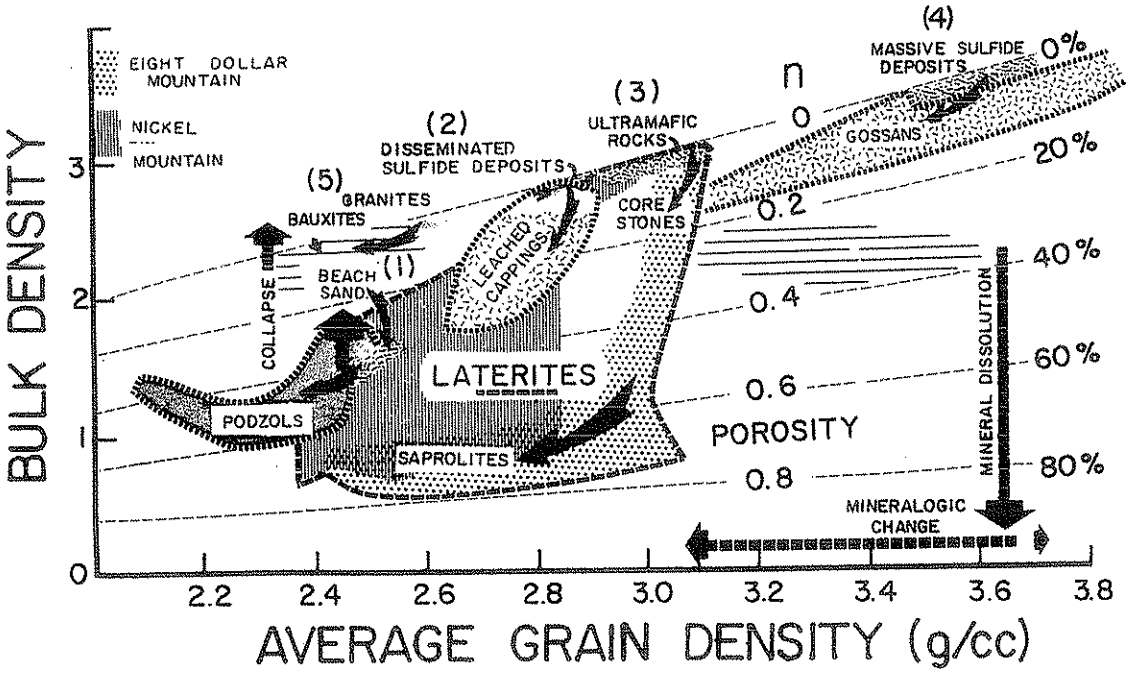

FIG. 17. Comparison of bulk density, grain density, and porosity of five protoliths and their chemical weathering products: (1) beach sand and podzols (this study); (2) disseminated sulfide ore deposits, *e.g.*, porphyry copper deposits and leached cappings (CUNNINGHAM, 1984); (3) ultramafic rocks and laterites (Fig. 5, this study); (4) massive sulfide deposits and gossans (from BLAIN and ANDREW (1977); and (5) granites and bauxites. Bauxites and gossans are shown only diagrammatically. Weathering paths of each hydrochemical system are indicated with arrows. The relative importance of pore creation by mineral dissolution, mineralogical change, and deformation (shown by straight dashed arrows) can be estimated from the shape and size of the field of weathering products in relation to the position of the protoliths. In the case of bauxites, minerals are formed during weathering which have a substantially higher density than their protolith phases. These are indicated crudely with a horizontal ruled pattern for highly porous boehmite deposits (NIA, 1968).

undergone chemical weathering to yield the expansive residual bauxite regions occurring as elongate belts on the southwestern and northeastern margins of the Australian continent. This inference is consistent with the numerous very large occurrences of mineable concentrations of rutile, ilmenite, and zircon and associated rare earth elements which are known in beach sands and recent sediments in coastal regions of Queensland and western Australia. It is inferred that these heavy mineral sands may have been derived from erosion of surficial weathering products enriched in phases resistant to chemical attack.

COMPARISON OF WEATHERING SYSTEMS

Comparison of the laterite and podzol systems presented here is made with three other types of chemical weathering systems of major importance in terms of density-porosity relations (Fig. 17). Here, the nature of five protoliths are shown: (1) porous beach sands, (2) disseminated sulfide ore deposits, (3) ultramafic rocks, (4) massive sulfide deposits, and (5) granitic basement protoliths for bauxites. Protoliths (4) and (5) are only indicated diagrammatically, as relevant data are scarce. Weathering products characteristic of each protore are shown: podzols, leached cappings, laterites, gossans, and bauxites. The shape and size of each field of weathering products can be used to infer the relative importance of mineral dissolution, mineralogical change towards lower or higher density phases, and deformation in the weathering paths shown. All five systems may be enriched by supergene processes, and differ mainly in the extent of residual enrichment and deformation. The extremely high porosities and low bulk densities attained in podzols and laterites may cause strong residual enrichment of immobile elements by factors exceeding five in the zone of leaching of mobile elements. Leached cappings and gossans, in contrast, are generally much less porous, are generally residually enriched to a lesser extent, and may be relatively undeformed. Bauxites, while only shown schematically in Fig. 17, present interesting effects which may in part run counter to the trends of the other systems, including the development of highly porous zones with high grain densities. In podzols, laterites, leached cappings, and gossans, weathering product minerals typically have grain densities which are less than those of the primary minerals. In contrast, certain portions of bauxite deposits, described at the Ketro Mine, Parnassus, Greece (NIA, 1968; VALETON, 1972) are dominated by diaspore (3.4 specific gravity) and are interpreted as desilicification and dehydration products.

CONCLUSIONS

Use of constitutive mass balance relationships offers a means of making unique inferences about the interrelated surficial processes involving aqueous fluid flow such as chemical weathering and geomorphic evolution. Chemical elements can be used to great advantage in understanding complex hydrochemical systems and the relationship of processes occurring at the surface to those immediately in the subsurface when their behavior patterns are rigorously assessed and their mobility interpreted. Most importantly, this approach helps to put chemical weathering and pedogenesis in a much needed quantitative framework, both for improving analytical description of natural systems and also in providing an essential basis on which to formulate hypotheses which can be tested and generalized.

Acknowledgements—We are grateful to NSF for Grant EAR-8416790 which provided this unique opportunity for our collaboration in the field and the support of the Earth Science Division of Lawrence Berkeley Lab. All photography was done by Joachim Hampel, who also performed the XRF analysis with exacting dedication to accuracy. His efforts are much appreciated. Professors Hans Jenny and Arnold Schultz kindly shared their time and experience with the authors at the Jug Handle Reserve where the podzol work has been done, and have continued to be a source of inspiration. Professor Charles Gilbert contributed his considerable petrographic skill to the analysis of heavy minerals in the podzols. The cooperation of Hanna Mining Company personnel, especially mine manager John Murphy and engineer Victor Mejia, as well as Jim Eidel of the Illinois Geological survey were invaluable. Mary Power cheerfully helped in the field sampling effort of the Eight Dollar Mountain laterite in Oregon. Tim Teague expertly made thin sections and probe mounts of difficult pedogenic materials. Discussions with Ron Amundson, Harvey Doner, and Gene Kelly provided useful perspectives on the podzol problem. Charlie Alpers provided useful data on massive sulfide densities. Simon Somers made most of the porosity and grain size analyses, and Chris Lewis helped with the XRF work and performed the AAS Fe analysis of podzols. Joan Bossart expertly handled the word processing. The final text has benefitted from helpful reviews by M. J. Pavich, D. Nahon and R. Stallard.

Editorial handling: G. R. Holdren, Jr.

REFERENCES

ALPERS C. A. and BRIMHALL G. H. (in press) Climatic desiccation—optimal hydrologic, geochemical, and geomorphic conditions for supergene enrichment and preservation of ore deposits: An integrated study of La Escondida, Chile. *Bull. Geol. Soc. Amer.*

ATHY L. F. (1930) Density, porosity, and composition of sedimentary rocks. *Amer. Assoc. Petr. Geol. Bull.* **14**, 1–24.

BLAIN C. F. and ANDREW R. L. (1977) Sulfide weathering and the evaluation of gossans in mineral exploration. *Min. Sci. Eng.* **9**, 119–150.

BRIMHALL G. H., ALPERS C. and CUNNINGHAM A. B. (1985) Analysis of supergene ore-forming processes using mass balance principles. *Econ. Geol.* **80**, 1227–1254.

BUOL S. W., HOLE F. D. and MCCRACKEN R. J. (1980) *Soil Genesis and Classification.* Iowa State University Press, Ames, Iowa, 404 p.

BUURMAN P. (ed.) (1984) *Podzols.* Van Nostrand Reinhold, New York. 450 p.

CHESWORTH W. and MACIAS-VASQUEZ F. (1985) Pe, pH, and podzolization. *Amer. J. Sci.* **285**, 128–146.

COEN G. M. and ARNOLD R. W. (1972) Clay mineral genesis of some New York spodosols. *Soil Sci. Soc. Amer. Proc.* **36**, 342–350.

CUMBERLIDGE J. T. and CHASE M. C. (1968) Geology of the Nickel Mountain Mine, Riddle, Oregon. In *Ore Deposits of the United States, 1933–1967* (ed. J. D. RIDGE). Graton-

Sales Volume, Amer. Inst. Mining Metall. Petr. Engineers, New York. 2, 1650–1672.

CUNNINGHAM A. B. (1984) Field and theoretical analysis of supergene processes: Ground water flow with chemical reaction in the weathering environment. M.S. thesis, Univ. California, Berkeley, 58 p.

ESSON J. (1983) Geochemistry of a nickeliferous laterite profile, Liberdale, Brazil. In *Residual Deposits: Surface Related Weathering Processes and Materials* (ed. R. C. L. WILSON), pp. 91–99. Geol. Soc. London Spec. Publ.

GOLIGHTLY J. P. (1979) Nickeliferous laterites: A general description. In *International Laterite Symposium* (eds. D. J. I. EVANS and R. S. SHOEMAKER), pp. 3–23. Soc. Min. Engineers, New York.

GOLIGHTLY J. P. (1981) Nickeliferous laterite deposits. In *Econ. Geol. 75th Anniv. Vol. (1905–1980)* (ed. B. J. SKINNER), pp. 710–734.

GRESENS R. L. (1967) Composition-volume relations of metasomatism. *Chem. Geol.* 2, 47–65.

GRUBB P. L. C. (1970) Mineralogy, geochemistry, and genesis of the bauxite deposits on the Gove and Mitchell Plateaus, northern Australia. *Mineralia Deposita* 5, 248–272.

GRUBB P. L. C. (1971) Genesis of the Weipa bauxite deposits, N.E. Australia. *Mineralia Deposita* 5, 265–274.

GRUBB P. L. C. (1979) Genesis of bauxite deposits in the lower Amazon basin and Guianas coastal plain. *Econ. Geol.* 74, 735–750.

HOLLAND H. D. (1984) *The Chemical Evolution of the Atmosphere and Oceans.* Princeton Univ. Press, Princeton, N.J., 583 p.

HOTZ P. H. (1964) Nickeliferous laterites in southwestern Oregon and northwestern California. *Econ. Geol.* 59, 355–397.

JENNY H. (1980) *The Soil Resource—Origin and Behavior.* Springer, Berlin and New York, 377 p.

JENNY H., ARKLEY R. J. and SCHULTZ A. M. (1969) The Pygmy Forest-podzol ecosystem and its dune associates of the Mendocino coast. *Madrona* 20, 60–74.

MEYER C., SHEA E. P., GODDARD C. C. JR. and staff (1968) Ore deposits at Butte, Montana. In *Ore Deposits of the United States, 1933–1967* (ed. J. D. RIDGE). Graton-Sales Volume, Amer. Inst. Mining Metall. Petr. Engineers, New York, 2, 1650–1672.

MILLOT G. (1970) *Geology of Clays: Weathering, Sedimentology, Geochemistry.* Springer, New York, 429 p.

NIA R. (1968) Geologische, petrographische, geochemische Untersuchungen zum Problem der Boehmit-Diaspor Genese in griechischen ober Kreidebauxiten der Parnaa-Kiona Zone. Thesis, University of Hamburg, Hamburg, 133 p.

RAMP L. (1978) Investigations of nickel in Oregon. *Misc. Paper* 20, Dept. of Geology and Mineral Industries, Portland, Oregon. 68 p.

RODE A. A. (1970) *Podzol-Forming Processes* (trans. from Russian), Academy of Sciences of the USSR, Dokuchaev Soil Science Institute, Leningrad, USSR. 387 p.

SADLEIR S. B. and GILKES R. J. (1976) Bauxite in relation to parent material. *J. Geol. Soc. Australia* 23, 333–344.

UGOLINI F. C., MINDEN R., DAWSON H. and ZACGARA J. (1977) An example of soil processes in the Abies Amabilis zone of the central Cascades, Washington. *Soil Sci.* 124, 291–302.

VALETON I. (1972) *Bauxites.* Elsevier, Amsterdam, 226 p.

VAN HOUTON F. B. (1982) Ancient soils and ancient climates. In *Climates in Earth History,* pp. 112–117. National Academy Press, Washington, D.C.

WILSON R. C. L. (ed). (1983) *Residual Deposits: Surface Related Weathering Processes and Material.* Blackwell, London, 259 p.

APPENDIX 1. Physical and chemical properties of samples from Eight Dollar Mountain, Oregon. Abbreviations of sample types are: sp = saprolite; sl = soil; cs = corestone; ccs = cored-corestone using 1-inch diamond drill to sample least altered interior portion of core stone; p,h = harzburgite protolith.

Sample Number	Pit Number	Depth (m)	ρ_w g/cc	ρ_g g/cc	$\frac{\rho_p}{\rho_w}$	$C_{Ni,w}$ %	$\frac{C_{Ni,w}}{C_{Ni,p}}$	Porosity n	Type	Surface Slope (degrees)
1100-08	4	2.13	0.98	—	3.01	1.22	4.69	—	sp	< 10
1100-09	4	2.95	1.00	2.87	2.95	1.20	4.62	0.65	sp	< 10
1100-10	4	1.07	1.49	2.90	1.98	0.62	2.38	0.49	sl	< 10
1100-11	4	1.31	1.14	2.87	2.59	0.88	3.38	0.60	sp	17
1100-12	4	1.31	1.18	2.81	2.50	0.96	3.69	0.58	sp	17
1100-13	4	2.84	2.62	—	1.10	0.31	1.19	—	cs	17
1100-14	4	2.84	0.99	2.40	2.98	0.79	3.04	0.59	sp	17
1100-15	4	2.77	1.21	2.91	2.44	0.69	2.65	0.59	sp	17
1100-16	4	0.37	1.22	2.99	2.42	0.78	3.00	0.59	sp	17
1100-17	4	2.99	3.00	3.04	0.98	0.41	1.58	0.02	cs	17
1100-17cs	4	2.99	3.22	—	0.92	0.31	1.19	—	ccs	17
1100-18	4	2.88	2.98	3.06	0.99	0.33	1.27	0.03	cs	17
1100-19	3	0.05	1.30	2.94	2.27	0.69	2.65	0.56	sl	10
1100-20	3	0.95	1.02	2.76	2.89	0.84	3.23	0.64	sp	10
1100-21	3	0.95	0.99	2.76	2.98	0.82	3.15	0.64	sp	10
1100-22	3	1.86	0.63	2.60	4.68	1.17	4.50	0.76	sp	10
1100-23	3	1.86	0.70	2.52	4.27	1.05	4.04	0.72	sp	10
1100-24	3	2.93	0.85	3.06	3.47	0.96	3.69	0.72	sp	10
1100-25	3	2.93	0.86	2.79	3.43	0.88	3.38	0.70	sp	10
1100-26	3	6.46	2.72	—	1.08	0.29	1.12	—	cs	10
1100-27	2	0.05	1.04	2.75	2.84	0.57	2.19	0.62	sl	6
1100-28	2	0.05	1.14	2.91	2.59	0.47	1.81	0.61	sl	6
1100-29	2	0.91	0.87	2.72	3.39	1.00	3.85	0.68	sp	6
1100-30	2	0.91	0.82	2.80	3.60	1.06	4.08	0.71	sp	6
1100-31	2	1.83	0.79	2.99	3.73	1.08	4.15	0.74	sp	6
1100-32	2	1.83	0.93	2.82	3.07	0.76	2.92	0.67	sp	6
1100-33	2	2.87	3.13	3.03	0.94	0.41	1.58	0.00	cs	6
1100-34	2	2.74	0.83	2.80	3.55	0.74	2.85	0.70	sp	6
1100-35	1	0.05	1.09	3.14	2.71	0.72	2.77	0.66	sl	21
1100-36	1	1.65	0.92	2.78	3.21	0.80	3.12	0.67	sp	21
1100-37	1	2.04	1.01	2.82	2.92	1.08	4.15	0.64	sp	21
1100-38	1	2.74	0.89	3.03	3.31	1.08	4.15	0.71	sp	21
1100-39	1	3.20	0.75	2.97	3.93	0.87	3.35	0.75	sp	21
1100-40	1	3.26	2.60	2.87	1.13	0.49	1.88	0.10	cs	21
1100-40cs	1	3.26	2.84	—	1.04	0.24	0.92	—	cs	21
1100-41	1	3.26	2.89	3.08	1.02	0.26	1.00	0.06	cs	21
1100-44		—	2.95	3.10	—	0.26	—	—	p,h	—

APPENDIX 2. Physical and chemical properties of samples from Nickel Mountain, Oregon. Abbreviations are the same as APPENDIX 1, except that p,p = peridotite protolith and p,d = protolith dunite.

Sample Number	Site Number	Depth (m)	ρ_w g/cc	ρ_g g/cc	$\frac{\rho_p}{\rho_w}$	$C_{Ni,w}$ %	$\frac{C_{Ni,w}}{C_{Ni,p}}$	Porosity n	Type	Surface Slope (degrees)
1100-1A	Pit	—	2.93	2.95	—	0.23	—	0.01	p,p	
1100-1B	Pit	—	3.04	3.06	—	0.24	—	0.01	p,p	
1100-1C	Pit	—	3.03	2.99	—	0.23	—	0.00	p,p	
1100-2A	Pit	—	2.81	2.85	—	0.32	—	0.02	p,d	
1100-2B	Pit	—	3.03	2.94	—	0.33	—	0.00	p,d	
1100-2C	Pit	—	2.95	2.91	—	0.32	—	0.00	p,d	
1100-45	1	0.20	0.92	2.85	3.26	0.55	2.36	0.68	sl	15
1100-46	1	0.59	0.80	2.71	3.75	0.79	3.39	0.70	sp	15
1100-47	1	0.59	0.84	2.68	3.57	0.73	3.13	0.69	sp	15
1100-48	1	1.18	0.59	2.56	5.08	0.91	3.91	0.77	sp	15
1100-49	1	1.18	0.72	2.46	4.17	0.86	3.69	0.71	sp	15
1100-50	1	1.76	0.72	2.40	4.17	0.76	3.26	0.70	sp	15
1100-51	1	1.76	0.75	2.44	4.00	0.76	3.26	0.69	sp	15
1100-52	1	2.45	1.85	2.47	1.62	1.00	4.29	0.25	cs	15
1100-52cs	1	2.45	2.86	—	1.05	0.41	1.76	—	ccs	15
1100-53	1	1.76	2.26	2.69	1.33	0.65	2.79	0.16	cs	15
1100-53cs	1	1.76	2.98	—	1.01	0.29	1.24	—	ccs	15
1100-54	2	1.66	0.70	2.50	4.29	1.36	5.84	0.72	sp	5
1100-55	2	1.66	0.70	2.38	4.29	1.41	6.05	0.71	sp	5
1100-56	2	2.76	0.87	2.47	3.45	0.86	3.69	0.65	sp	5
1100-57	2	2.76	0.67	2.46	4.48	1.03	4.42	0.73	sp	5
1100-58	2	3.87	2.02	2.84	1.49	0.67	2.92	0.29	cs	5
1100-58cs	2	3.87	2.39	—	1.25	0.29	1.24	—	ccs	5
1100-60	2	—	—	—	—	—	—	—	—	—
1100-61	3	0.34	0.82	2.77	3.66	0.84	3.61	0.70	sl	20
1100-62	3	3.49	0.83	2.67	3.61	1.60	6.87	0.69	sp	20
1100-63	3	3.49	0.89	2.68	3.37	1.51	6.48	0.67	sp	20
1100-64	3	1.59	0.85	2.61	3.53	1.29	5.54	0.68	sp	20
1100-65	3	1.59	0.82	2.68	3.66	1.74	7.47	0.69	sp	20
1100-66	3	2.27	1.05	2.45	2.86	1.55	6.65	0.57	sp	20
1100-67	3	2.27	1.49	2.22	2.01	1.51	6.48	0.33	cs	20
1100-68	4	0.05	0.97	2.78	3.09	0.88	3.78	0.65	sl	28
1100-69	4	2.49	1.08	2.48	2.78	0.81	3.48	0.57	sp	28
1100-70	4	2.49	0.95	2.54	3.16	0.53	2.27	0.63	sp	28
1100-71	4	3.32	0.86	2.46	3.49	0.78	3.35	0.66	sp	28
1100-72	4	3.32	0.94	—	3.19	0.86	3.69	0.62	sp	28
1100-73	4	3.87	2.58	2.88	1.16	0.54	2.32	0.11	sp	28
1100-74	4	2.84	2.31	2.69	1.30	0.74	3.18	0.14	cs	28
1100-75	4	2.96	1.09	2.48	2.75	0.72	3.09	0.56	sp	28
1100-76	4	3.18	2.48	2.38	1.21	0.81	3.48	0.00	cs	28
1100-76cs	4	3.18	2.72	—	1.10	0.57	2.45	—	ccs	28
1100-77	4	3.26	0.92	2.42	3.26	0.91	3.91	0.62	sp	28

APPENDIX 3. Physical and chemical data for the Pygmy Forest podzols. Soil types are shown in Fig. 9 using the scheme of BUOL *et al.* (1980). Protolith beach sands from Terrace 1 near the coast are indicated by a (p) (samples 1107-28,29,30). All analyses are by XRF, Joachim Hampel analyst, using pressed pills for traces and minor elements, fused glass plates for major elements.

Sample Number	Depth (m)	ρ_w	ρ_g	$\frac{\rho_p}{\rho_w}$	Porosity n	Type	Fe %	Al %	Ga (ppm)	Cu (ppm)	Pb (ppm)
1107-01	1.57	1.17	2.46	1.32	0.53	B2'ir	7.50	9.29	12.0	34.1	35.8
1107-02	1.64	1.44	2.08	1.07	0.31	B2'ir	6.95	8.42	9.3	24.0	28.0
1107-03	1.72	1.05	2.44	1.47	0.57	B2'r	4.40	6.51	7.6	28.8	27.5
1107-04	0.05	0.96	2.24	1.61	0.55	A1	0.089	0.476	0.0	7.8	10.3
1107-05	0.24	1.81	2.42	0.85	0.26	E	0.090	0.037	0.0	0.0	10.6
1107-06	0.14	1.38	2.35	1.12	0.42	A1	0.022	0.261	0.0	0.0	11.0
1107-07	0.24	1.79	2.52	0.86	0.29	E	0.32	0.274	0.0	2.8	10.6
1107-08	0.14	1.17	2.32	1.32	0.46	A1	0.45	0.267	0.0	0.0	11.8
1107-09	0.36	1.30	2.09	1.19	0.38	A3	0.89	4.52	10.3	8.9	21.4
1107-10	0.43	1.68	2.45	0.92	0.32	B mir	0.61	2.21	9.3	6.2	18.5
1107-11	0.43	1.65	2.49	0.94	0.34	B mir	0.44	1.94	5.9	8.6	15.8
1107-12	0.43	1.82	2.50	0.85	0.27	B mir	0.53	2.28	6.2	2.4	16.9
1107-13	0.65	1.73	2.51	0.89	0.31	E'x	0.077	0.332	2.0	0.0	10.2
1107-14	0.89	1.08	2.26	1.43	0.52	B'1	2.23	11.5	77.0	24.5	46.7
1107-15	1.08	1.23	2.24	1.26	0.45	B2'ir	8.05	11.1	9.5	20.1	28.4
1107-16	1.03	1.30	2.46	1.19	0.47	B2'ir	8.28	12.5	13.7	39.1	36.3
1107-17	0.67	1.86	2.51	0.83	0.26	E'X	0.10	0.337	—	—	—
1107-28	—	1.43	2.48	—	0.43	p	0.62	2.66	3.5	4.9	17.9
1107-29	—	1.58	2.50	—	0.37	p	0.57	3.10	4.4	10.7	17.0
1107-30	—	1.63	2.53	—	0.36	p	0.63	2.80	2.8	8.4	22.6